Keck Adaptive Optics Note 685

NGAO Optical Relay Design

Renate Kupke and Chris Lockwood

Revision History:
Version 1: Oct 27, 2010
Version 2: May 18, 2010
Version 2.1: June 2, 2010

Table of Contents

1. Introduction

This document presents the preliminary optical design for the Keck Next Generation Adaptive Optics Relay. The design is based on results of the conceptual design study, KAON 549, and subsequent build-to-cost reductions and guidelines. Section 2 of this document outlines some of the main requirements the optical design must satisfy. Section 3 describes the components of the optical relay in more detail, and in Section 4 the performance of the relay with regard to science instruments and wavefront sensors is discussed.

2. Design Choices and Requirements

The requirements, as defined in KAON 549 for the conceptual design, have altered somewhat due to build-to-cost design changes in KAON 642. The current requirements include, but are not limited to:

- Location:
  - The AO system will reside on the left Nasmyth platform. (SR-744)
- Wavelength Range
  - The AO relay shall transmit a wavelength range of 0.818μ - 2.4μ for the NIR imager (INT 157) and NIR integral field spectrograph (INT-382).
  - The AO relay shall transmit 1.16-1.77μ to the LOWFS (FR-175) and shall not preclude K-band
  - The AO relay shall transmit 1.1-4.1μ to the interferometer (SR-683).
  - The NGS WFS will require 0.4-0.8μ light (FR-140 and KAON 642).
  - THE LGS WFS will require 589nm sodium light (FR-523).
- Field of View:
  - A high-Strehl science relay with an unvignetted field of view (FOV) of at least 20 arcseconds diameter with a goal of 40 arcseconds diameter. (FR 41)
  - A 120 arcsecond diameter field of regard (FOR) at the focal plane of the first relay, providing natural guide stars (NGS) for the low-order wavefront sensors (LOWFS). (FR 40)
  - A 120 arcsecond diameter unvignetted FOR for guidestars from 80 to 270 km in altitude to the LGS WFS (FR 1980, FR 1869).
  - The NGS WFS shall be able to acquire any guide star in a field of view of 40” x 60” (FR 127).
- Entrance Window
  - The entrance window shall provide a thermal seal between the cold enclosure of the AO system and the ambient room temperature. It shall consist of two windows to prevent condensation, and it shall be big enough to transmit the entire 120” field of view (FR 1888).
- Field and Pupil Rotation:
  - The optical relay will have a K-mirror upstream of the science instruments and wavefront sensors that can pass the entire field of view (FR 31).

- Deformable mirrors
  - The wide field relay shall contain a deformable mirror conjugate to the telescope pupil, with a pupil size of 100mm. The deformable mirror shall have 20 actuators across the pupil diameter. (FR-32 and FR-56). The requirements do not state whether this is circumscribed pupil diameter, maximum mirror diameter, active mirror area, or mirror area, however, the arrangement in drawing NGAO/ConfigControl/1410-CM0010 (see also Figure 18 and Figure 19) shows a configuration designed to allow for telescope pupil notation, and used as the guideline for beam sizes in the AO relay design.
  - The narrow field relay shall contain a deformable mirror conjugate to the telescope pupil with a pupil size of 24mm. The deformable mirror shall have 60 actuators across the pupil diameter. (FR-33 and FR-57).
- Output pupil location:
  - The exit pupil for the first relay will be telecentric to simplify design of the LOWFS pick-off mechanisms. (FR-1502)
  - The exit pupil for the entire relay will be telecentric to simplify design of the NGS WFS. (FR-1501)
- Output focal ratio:
  - The output focal ratio of the first relay shall be the same as the input focal ratio of the telescope, and shall be made compatible with the input for the LOWFS, the second relay, the acquisition camera, and the interferometer. (F-1499)
  - The output focal ratio of the second relay shall be greater than f/40 . (FR-1500) There is no requirement stating the upper bound for the output focal ratio.
- Optical Switchyard
  - The relay design should provide for a LGS WFS sodium dichroic (FR-67), a removable NGS WFS dichroic (FR-39), and a removable acquisition camera fold (FR-68). There are currently no requirements for instrument selection.

3. First-Order Optical Layout

An annotated optical layout is shown in Figure 1. The following sub-sections describe each component of the optical relay in detail.

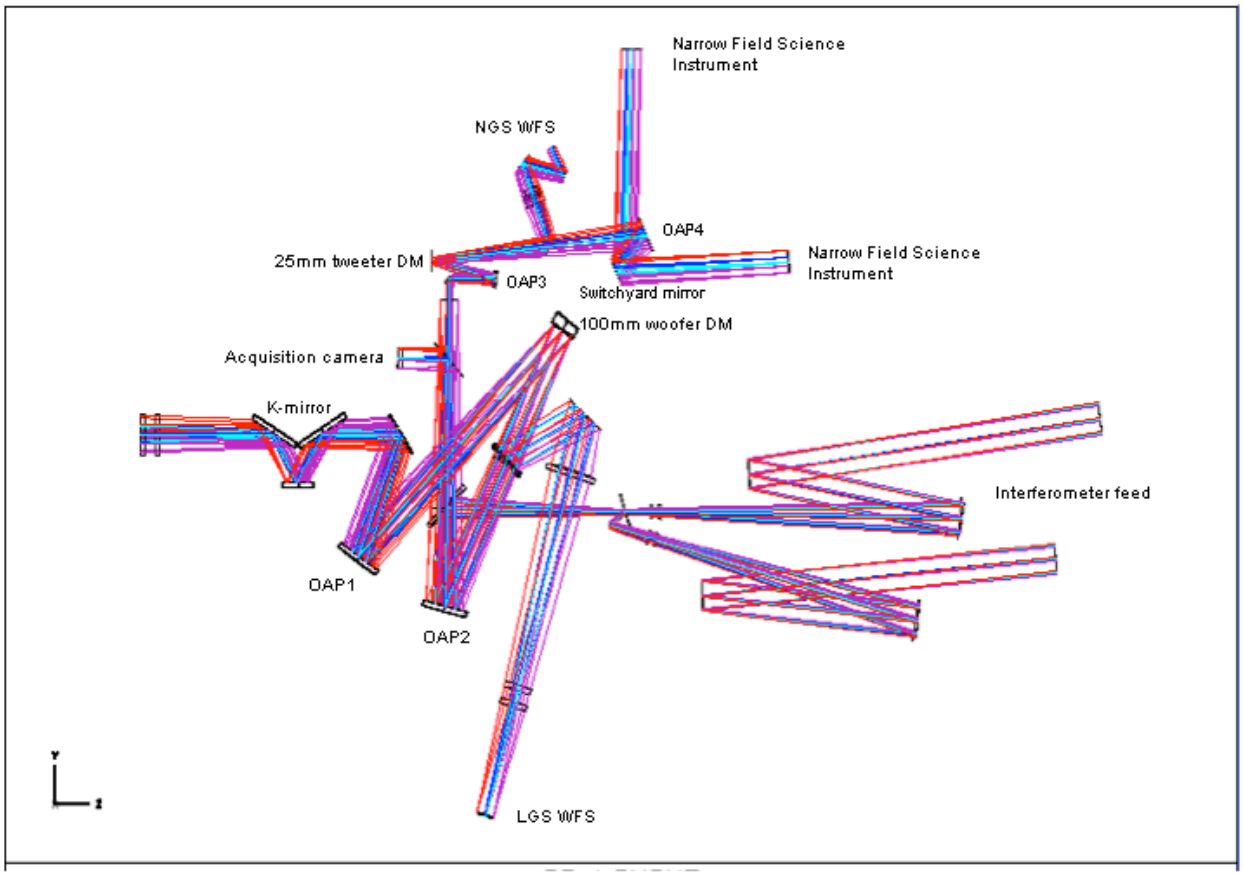

Figure 1. Annotated optical layout of the AO relay. Light from the telescope tertiary mirror enters from the left. The first, f/13.66 matched-OAP relay contains a 100mm low order DM conjugate to the telescope primary. The second, f/46.38 OAP relay contains the 25mm MEMs high order DM conjugate to the telescope primary. The LGS dichroic picks off laser light, which is directed to the LGS WFS. Pick-offs for the low-order wavefront sensors (LOWFS) lie at the focal plane of the f/13.66 relay, and are not shown in this figure. There are also removable dichroic beamsplitters for the interferometer, the acquisition camera, and the natural guide star wavefront sensor.

3.1 Entrance Window

Because the AO relay is located in a temperature-controlled environment, sealed entrance and exit windows are required to isolate the AO bench from the ambient air. The entrance windows of the AO system are double-paned to prevent condensation, with dry nitrogen at air pressure between the two panes. The front face of the first window lies 795 mm before the telescope focus. Each of the 180 mm diameter windows is 25 mm thick. They are made of CaF2 substrate and coated with a broadband AR coating which will give good transmission from 0.4 -2.4 μ. This will likely be a Sol Gell coating and can be done by the Lick Coating lab.

3.2 K-mirror Rotator

The Nasmyth focus lies between the first and second mirrors of the K-mirror assembly (K1 and K2, respectively). The focal plane is located 121 mm after K1. The location of the focus is placed within the K-mirror to provide adequate space for the first off-axis parabola (OAP) of the relay, as described in the next section. The existing Keck AO relay has the first element of the K-mirror positioned after focus. The decision to move the focus to a point within the K-mirror assembly was based on the need to accommodate a smaller low order DM (100mm versus the existing 140mm diameter), and thus a shorter focal length OAP1.

The K-mirror consists of 3 mirrors, the first and third being tilted at 60 and -60 degrees, respectively, to the Nasmyth optical axis. The tilt angles are identical to the present Keck AO K-mirror assembly. The mirror diameters (assuming a 90% clear aperture) are as follows: K1=250 mm, K2=160 mm, and K3=270 mm. K1 is slightly larger than the present Keck AO K-mirror's K1 because of the need to pass both the LGS and NGS 120 arcsecond diameter FOV. K2 is the same size as the existing K2, and K3 is slightly smaller. The distance between K1 and K2, and K2 and K3, is 243.5 mm, as in the existing Keck image rotator. The mechanical design of the K-mirror assembly can therefore be very similar to that of the existing K-mirror. The K-mirror assembly was matched to that of the existing Keck system in an effort to maintain the polarization characteristics, in consideration of interferometer operation. It is therefore also desirable to match the coating of the new K-mirror to that of the K-mirror on the other Keck telescope. Presently, this would require a bare aluminum coating on the K-mirror or a recoating of the existing K-mirror.

3.3 First Relay

The first relay consists of two matched off-axis parabolas, the first of which produces, in collimated space, a plane conjugate to the primary mirror at which the 100 mm low order DM is placed. In the collimated space after the 100 mm diameter deformable mirror lies a dichroic designed to reflect laser guide star light (589 nm) to the LGS WFS, and transmit all other wavelengths. The second OAP of the matched-pair relays the Nasmyth focus to a second focal plane, preserving the f-number of the input beam. In the converging light following OAP2 are removable pick-offs to the interferometer and acquisition cameras.

For packaging, an additional fold mirror is needed in the diverging optical space following the K-mirror. This fold mirror lies 397.5 mm after K3, with an incidence angle of 34.5° and a diameter of 190 mm. The present Keck AO relay contains a similar fold mirror, which is used also as a tip-tilt steering mirror. It was decided not to incorporate this fold as a tip-tilt location, as its conjugate location is 22 km above the telescope, and a location conjugate to the telescope pupil was preferred to stabilize the pupil and to lessen the stroke requirement of the tip/tilt stage.

OAP1 has an apparent focal length determined to meet the requirement of a 100mm pupil on the low order DM by the following equation:

$$F_{OAP} = \left[\frac{d_{DM}}{d_{PM}}\right] F_{tel} \qquad (1)$$

where d_{DM} and d_{PM} are the diameters of the deformable mirror (100 mm) and the telescope primary (10.949 m), respectively, and F_{tel} is the focal length of the telescope (149.583 m). This gives an apparent focal length for OAP1 of 1366.2 mm.

The low order DM follows OAP1, at a distance from OAP1 conjugate to the telescope primary mirror:

$$t_{OAP1\to DM} = \left(\frac{-1}{t_{pupil} + F_{OAP1}} + \frac{1}{F_{OAP1}} \right)^{-1}, \qquad (2)$$

where t_{pupil} is the distance to the telescope exit pupil from telescope focus. Equation (2) gives a total OAP1 to woofer DMlow order DM distance of 1460 mm.

The focal lengths and distances derived above are derived assuming the parabola is used on-axis. The parent focal lengths of the off-axis parabolas were determined in Zemax given the off-axis distance and desired pupil size, are are F_{OAP1}=F_{OAP2}=1276.75 mm.

The low order DM is nominally 22x22 actuators (5mm pitch), and will be mounted on a real-time, tip-tilt platform. The pupil imaged on the low order DM is 100 mm, and therefore maps to 20x20 actuators of the 22x22 actuator device. Due to the incident angle of 10° the pupil will be elongated by 1.54% in one direction, and the beam footprint will be 101.5 mm in that direction.

In collimated space, 625 mm after the low order deformable mirror, lies the dichroic beamsplitter that will pick off the 589 nm light of the sodium LGS and direct it to the LGS WFS. This beamsplitter has an incidence angle of 19° to the optical axis, and a diameter of 190 mm.

Following the low order DM is OAP2, an off-axis parabola whose parameters exactly match those of OAP1 to minimize aberrations at infinite conjugate. It is located one focal length away from the low order DM, projecting the pupil to infinity and providing a telecentric beam for the second and LOWFS relays. A telecentric system was chosen to simplify the design of the LOWFS pick-off mechanisms and wavefront sensors. A telecentric system does not require tilt with field to keep the chief ray constant on entering the wavefront sensor. There are also no pupil scale changes with conjugate distance for the LGS WFS.

3.4 Tip-tilt platform

During the preliminary design stage, inquiries were submitted to vendors regarding the mounting of the low order deformable mirror on a fast tip-tilt stage. Primarily, we desired a comparison between the performance and cost of mounting a 100 mm diameter piezo-electric DM versus the larger 140 mm diameter DM. CILAS provided information about the SAM 416 (Gemini 4.5) and the SAM 349 (GTC) deformable mirrors, shown in

Table 1. These two mirrors are similar to our requirements for 100 mm and 140 mm low order DM.

Table 1. Characteristics of existing CILAS DMs.

DM	# actuators	pitch	aperture	Max	weight	volume
SAM 416	416	5.0mm	106mm	7.8μ	6.5kg	15x16x10cm^3
SAM 349	349	7.0mm	140mm	8.4μ	14.4kg	22x22x20cm^3

The mirrors listed in the table above were not intended for mounting on a tip/tilt platform. CILAS estimated that the weight of these DMs could be decreased by as much as 20% by changing the mechanical packaging in consideration of the tip-tilt platform mounting. When contacting the vendors the specifications included a 38.5Hz closed-loop bandwidth (the most stringent tip-tilt bandwidth requirement contained in the science cases), and the ability to compensate for the ~30Hz telescope vibration in an as-yet-unspecified feed-forward fashion.

The requirements database indicates a 3 arcsecond stroke is required on the tip/tilt platform (SR 688). At the tip/tilt platform at the low order DM this corresponds to

$$\alpha_{TT} = \left(\frac{F_{Tel}}{F_{OAP1}} \right) \alpha_{Sky},$$

where α_{Sky} is the 3 arcsecond stroke requirement on the sky, F_{Tel} is the focal length of the telescope and F_{OAP1} is the focal length of OAP1. This results in a α_{TT} of 1.6 milliradians peak-to-peak. Momentum compensation was also required to minimize vibration on the optical table.

Three vendors responded positively: CILAS, Physik Instrumente, and Left-hand Design. The bandwidth requirements, considering the weight and dimensions of the deformable mirror, are challenging. Table 3 summarizes the results of the inquiry. Physik Instrumente and Left Hand design indicated that the 140mm, with its 14.4kg weight, would be difficult to achieve at the specified bandwidth. CILAS, although not giving exact bandwidth values, suggested the 140mm diameter mirror would operate at a 30% decreased bandwidth over the 100mm. For this reason, the 100mm DM was chosen as baseline for the AO relay design.

Table 3. Results of initial vendor inquiries into tip/tilt stage

	CILAS	PI	Left-hand Design
Predicted achievable bandwidth	Has reached 50Hz on the TMT prototype	200Hz resonant frequency, claims 50Hz closed-loop	Open-loop servo control: Phase 1:20Hz, Phase 2: 50Hz, Phase 3 100Hz, Phase 4 200Hz
Sensor		Capacitive	
Type	Voice coil	Piezo	Voice coil

3.5 Laser Guide Star WFS

As illustrated in Figure 1, between the low order DM and OAP2 is a fixed dichroic beamsplitter to reflect sodium guide star light to the LGS WFS. The dichroic was placed in space that is

collimated for the science beam to minimize aberrations in the science and LOWFS beams. The LGS WFS does not receive a performance benefit from the matched OAPs due to the finite location of the laser guide star objects, nor is this space collimated for the laser guide star light. The laser guide star light does not share the same static aberrations as the science and LOWFS stars, so no loss in performance or significant increase in calibration complexity is incurred by using a separate focusing element for the laser guide stars.

The dichroic pick-off will ideally be a notch filter, reflecting only the sodium LGS wavelength of 589nm. A notch filter was chosen to allow visible light below 600nm to be available to the visible truth wavefront sensor (TWFS) located in the LOWFS assembly, and the NGS WFS. The dichroic has an incidence angle of 19°. The optical layout for only the LGS WFS section of the AO relay is shown in Figure 3. The LGS WFS dichroic lies downstream of the low order DM, so the LGS WFS will operate in closed-loop. Following the dichroic pick-off is a 250 mm diameter fold mirror. The fold mirror was added to locate the NGS WFS on the side of the AO system opposite the science output beam, in order to leave adequate space for two science instruments.

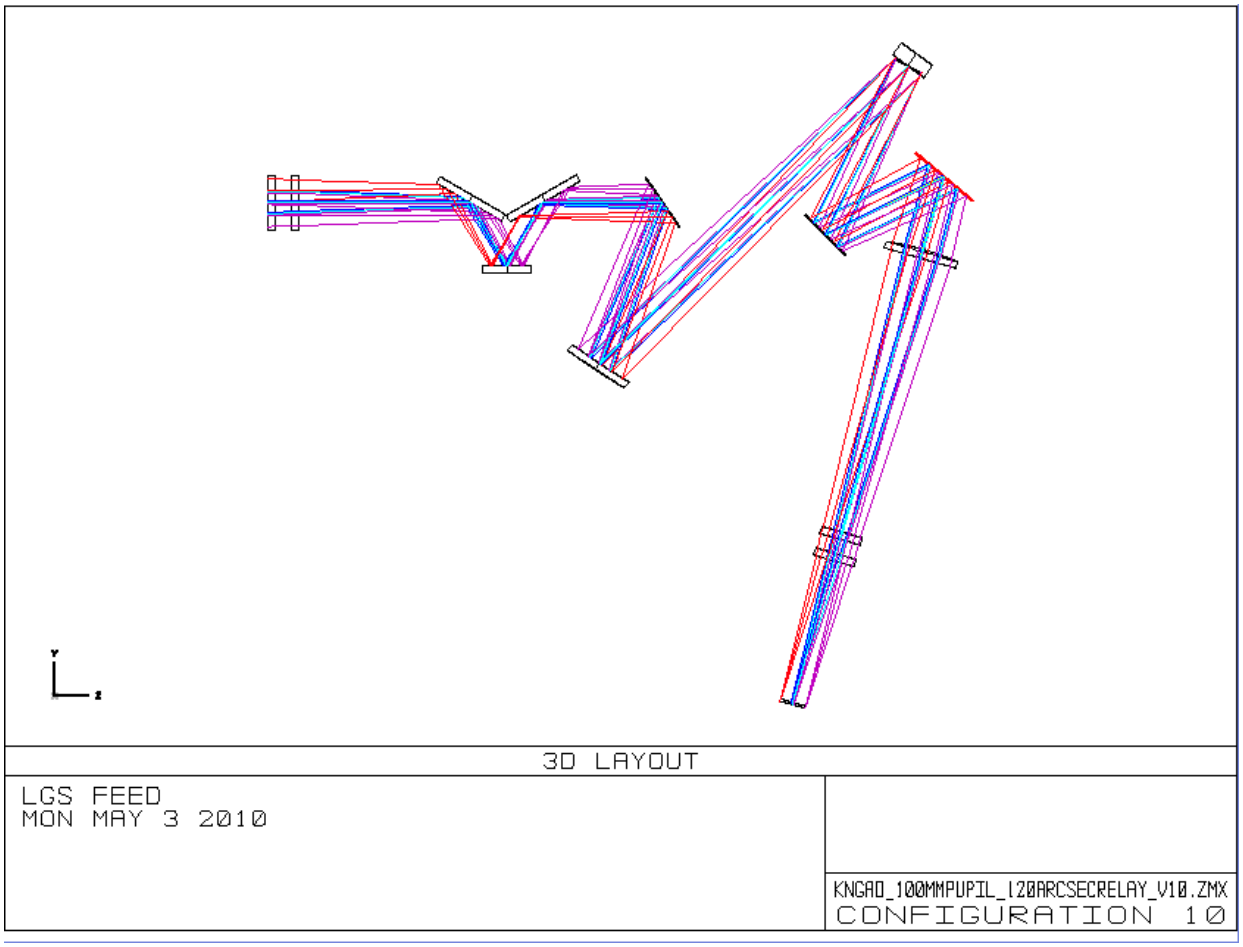

Figure 3. The LGS WFS optical relay.

The object selection mechanism (OSM) for the LGS WFS requires a focal plane, thus the collimated light reflected from the LGS dichroic is brought to focus by a single glass plano-

convex lens. Zemax modeling indicates that this lens will produce less wavefront error if the convex surface is an asphere. The decrease in RMS wavefront error with an aspheric surface over a spherical surface is 14%. The lens is located one focal length away from the low order DM, to provide a telecentric beam for the LGS OSM and relays. The output f/# of the LGS feed is approximately f/13.4.

In the converging beam, 950 mm after the plano-convex lens, is the 140 mm diameter double-paned exit window. The exit window need only transmit sodium wavelengths, so an AR-coated inexpensive crown glass such as BK7 should suffice.

3.6 Interferometer Feed

Located 500 mm after OAP2 is a removable dichroic available to feed the Keck interferometer (Figure 5). The interferometer utilizes J and H-band light for internal tracking (the J-band used primarily when doing H-band interferometer science). The interferometer dichroic will reflect J, H, K, and longer wavelength light, up to the required 4.1μ, to the interferometer. The LOWFS will not be used during interferometer operations. Instead, the NGS WFS will be configured to act as a LOWFS. The dichroic has an incidence angle of 42.75° and a diameter of 190 mm. A wedge of 0.17° on the second surface of the dichroic removes lateral color at the NGS WFS.

The interferometer dichroic directs the starlight to two field-steering mirrors. One of the mirrors has a hole which allows the on-axis light to pass straight through, while off-axis light is directed to the second field selection mirror. The beams exit the cold enclosure through CaF2 window(s) located after the field selection mirror. Both diverging beams are collimated with OAPs which are identical in diameter, focal length, and off-axis angle to the existing Keck DSM collimating OAPs. The collimated beams are directed to two steering dichroics, which both direct light to down-looking mirrors feeding the existing Nasmyth interferometer path, and provide light to diagnostic sensors located behind the dichroics. Figure 5 illustrates the interferometer optical path.

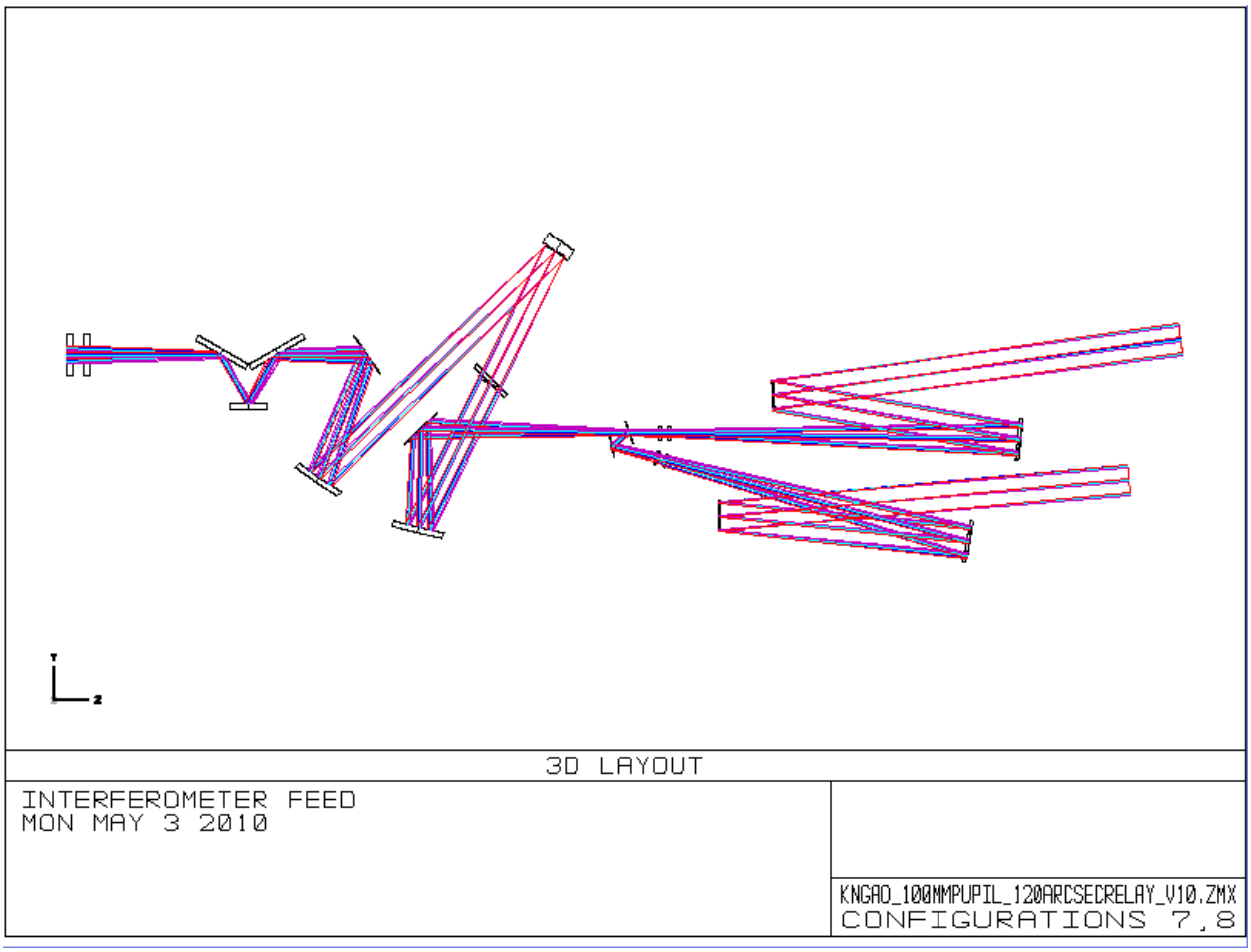

Figure 5. Relay showing interferometer reflective dichroic, field selection mirrors, collimating OAPs and fold dichroics of the Dual Star Module bench.

3.7 Wide-Field Relay to Acquisition Camera and LOWFS.

After the dichroic LGS WFS pick-off, the beam is refocused by OAP2 to produce an f/13.66 focal plane at the LOWFS pick-off plane. Located 250 mm before the focal plane is a removable dichroic, allowing a 90° reflection to an acquisition camera. Interferometer operation requires the dichroic to reflect 470 nm LED light to the acquisition camera while transmitting the rest of the visible band to the NGS WFS. Because the acquistion camera is also used for sodium guide star acquisition, the dichroic will transmit 600 – 800 μ to the NGS WFS. The acquisition camera will obtain images of the entire 120 arcsecond diameter field and allow acquisition of the natural guide stars for the LOWFS and an initial acquisition of the LGS. The LOWFS focal plane and acquisition camera pick-off are shown in Figure 6.

For the mechanical envelope, we have assumed that the acquisition camera design will be similar to the existing MAGIQ guider camera design, adapted to accommodate a slightly smaller field of view (2 arcminutes versus 3 arcminutes for the existing MAGIQ design). The acquisition camera must translate as a unit (field and camera lenses, as well as detector) to refocus up to 250 mm for the LGS acquisition.

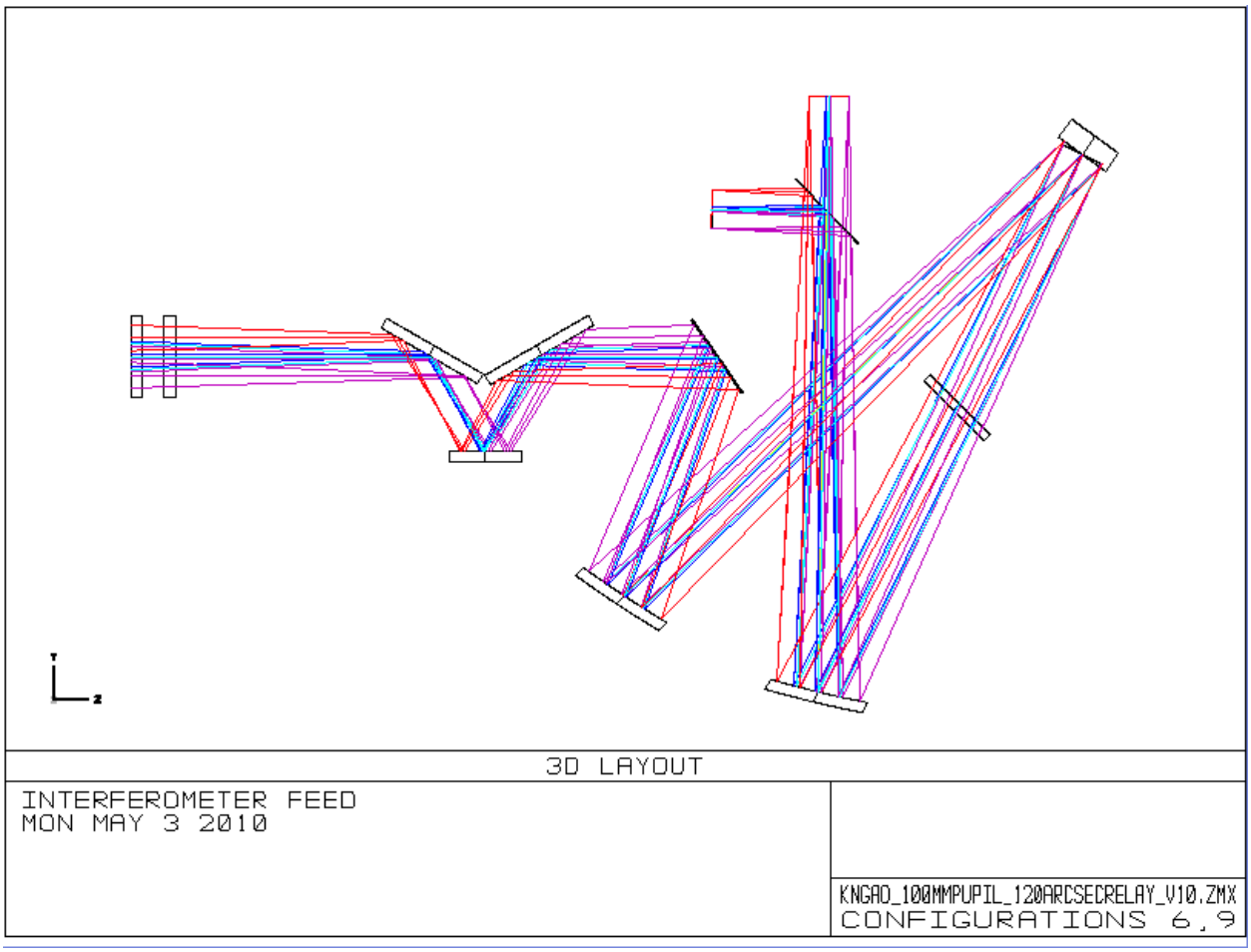

Figure 6. Wide-field relay, passing 120 arcseconds to tip-tilt sensors and low-order wavefront sensors. A removable dichroic provides the acquisition camera with the entire 120 arcsecond field of view.

3.8 Narrow-field, High Strehl Relay

Within the plane of the LOWFS pick-offs will be an unobstructed aperture to pass a 40x60 arcsecond rectangular field of view to a narrow-field, high Strehl relay. Although the science instruments require only a 40 arcsecond field of view (FOV), the larger 40x60 arcsecond rectangle was chosen to increase the patrol field of the natural guide star wavefront sensor. The optical path is shown in Figure 7. Directly after the focal plane, a fold mirror directs the light at 90° to its original direction to allow space for following optics (specifically the MEMs deformable mirror package) within the LOWFS pick-off mechanisms.

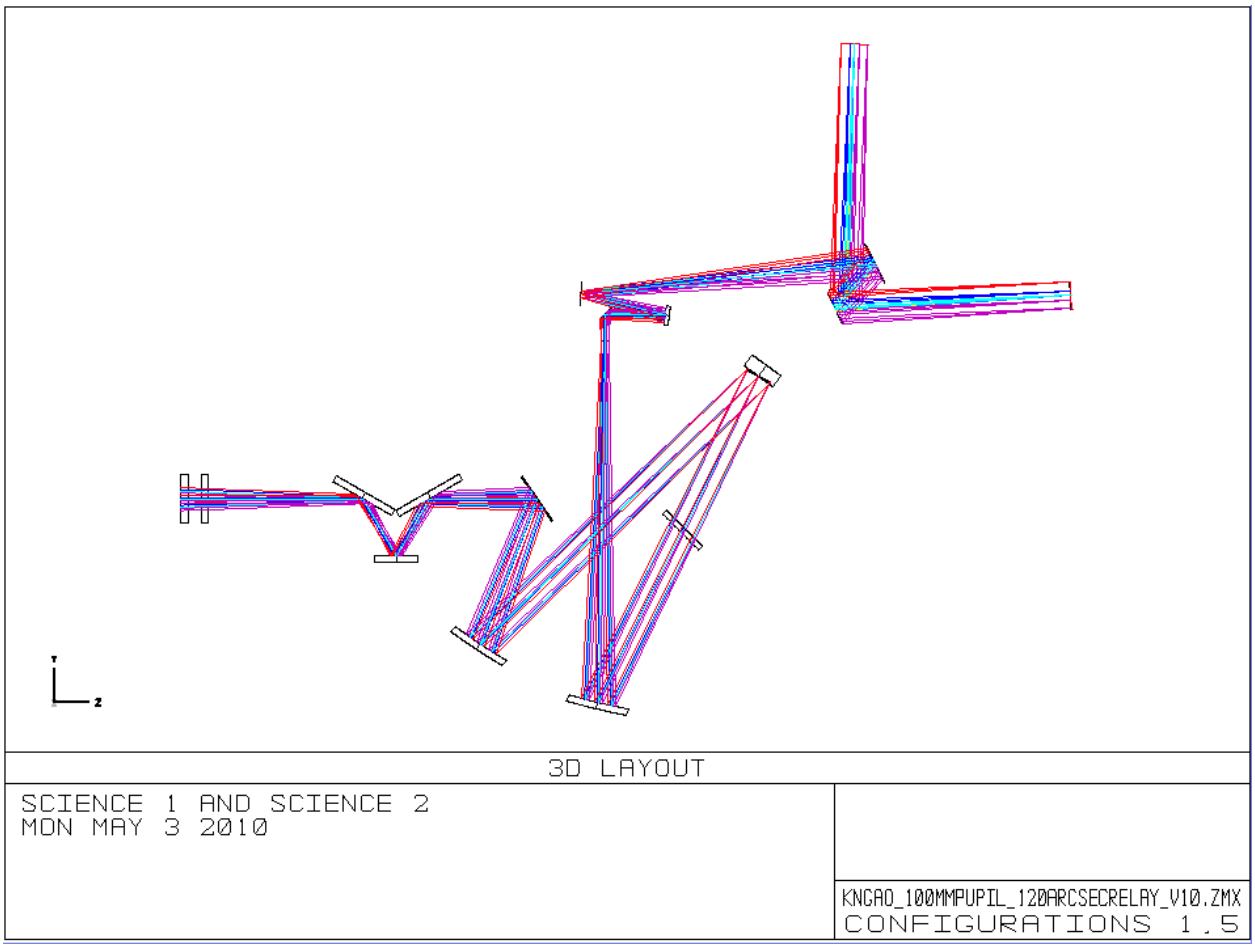

Figure 7. Two narrow-field science instruments are fed by the second OAP relay, which contains a high-order DM conjugate to the telescope pupil.

The narrow-field relay consists of two unmatched OAP mirrors producing a 24 mm pupil image on the high order DM and an output beam to feed the NIR imager, the integral field spectrograph (IFS) and a future unspecified science instrument.

The high order deformable mirror is a 64x64 actuator MEMs device with 0.4mm actuator centers. The 24 mm diameter pupil image on the high order DM will utilitize 60x60 actuators of the DM. The high order DM has an incidence angle of 10°, producing an elongation in one direction of 1.54% (24.4 mm). The MEMs device will be mounted on a "slow" tip-tilt stage, as discussed in KAON 669, to provide a steering mirror that can be used for dithering, differential tracking, compensation of differential atmospheric refraction, or fine guidance and centering on a spaxel or detector. The performance requirements of this steering platform are outlined in KAON 669.

Using Equation (1), we can determine the first order focal length of the OAP needed to produce a collimated beam with a 24mm telescope primary image on the high order DM (this corresponds to 60x60 subapertures). In this case, we substitute F_{OAP2} for F_{tel} and d_{DM1} for d_{PM}, to get F_{OAP3}=327.9mm. At an off-axis angle of 13° this corresponds to a parent focal length of 318

mm. The output of the first relay is telecentric, so the high order DM lies F_{OAP3} away from OAP3. The requirement FR-1500 dictated a focal ratio greater than f/40 for the beam exiting the relay, in order to provide space for an optical switchyard and instruments. F_{OAP4} was chosen in consultation with the mechanical engineering team to provide adequate space for the science instruments. The output beam of the relay is f/46.38. OAP4 is located exactly one focal length away from the high order mirror, to provide a telecentric beam for the instruments. To obtain the optimum image quality, the off-axis angle of OAP4 must increase by roughly the same factor as the magnification of the unmatched relay (see Ghedina and Ragazzoni 1997). Thus OAP4 has an off-axis angle of 41.9°, and a parent focal length of F_{OAP4}=953.96 mm.

A switchyard mirror, 350 mm beyond OAP4, directs the beam to the science instrument(s). The incident angle of the mirror is 20°.

A removable dichroic is located 727 mm beyond the high-order deformable mirror, with an incidence angle of 30°. The dichroic is located in a collimated beam, and a triplet produces an f/20 beam which is steered by two fold mirrors into the NGS WFS (see Figure 8). The triplet, designed by Velur, consists of BASF2, N15, and BASF2 glasses. Figure 8 shows the path of the NGS WFS pick-off.

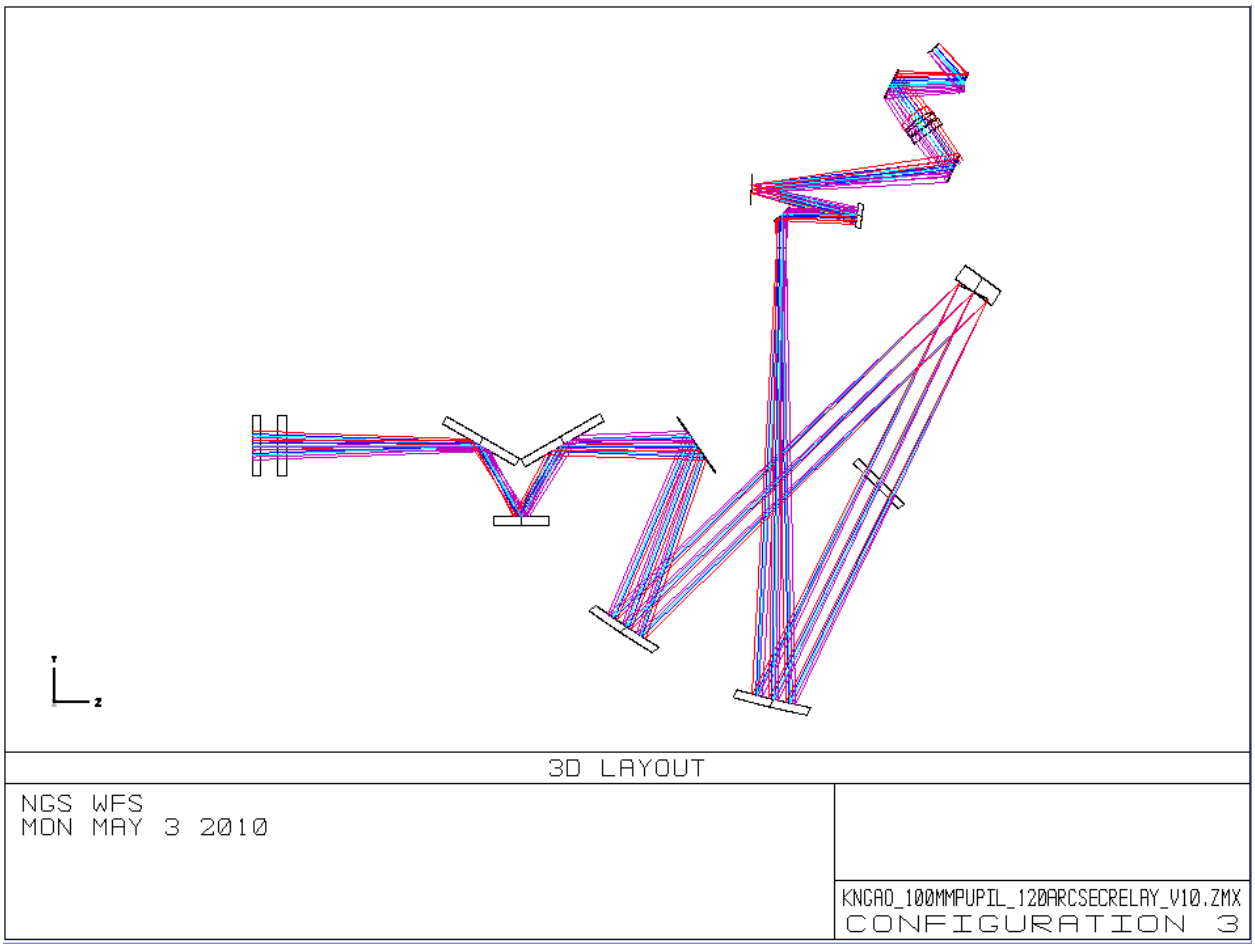

Figure 8. The relay to the NGS WFS, where a dichroic in the collimated space directs the beam to a triplet which produces an f/20 beam for the NGS WFS.

A patrol field larger than the science FOV was desired for the NGS WFS.A diagram of the field, and its relation to the science and LOWFS fields, is shown in Figure 9. The first relay fold mirror is sized to accommodate a 40x60 arcsecond field of view, the 60" in the direction perpendicular to the optical bench. OAP3 is circular, and sized to accept a field of diameter 60". The footprint of the 40"x60" rectangular field on OAP3 is shown in Figure 10.

It has also been proposed that the NGS WFS could act as a LOWFS when the observer requires the science object as a wavefront sensor reference in fixed pupil mode (see KAON 666).

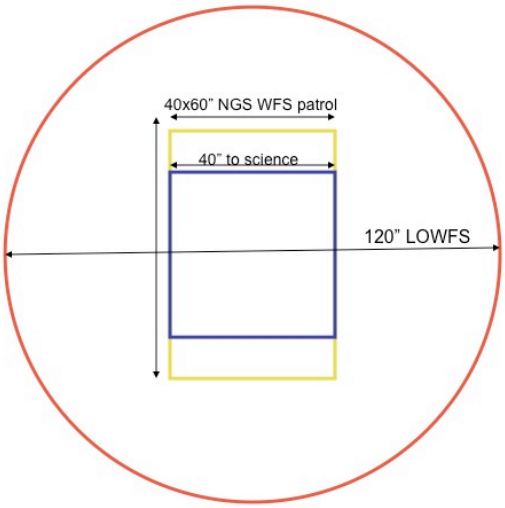

Figure 9. Outline of respective fields of view. The 120" diameter LOWFS patrol field (red), the rectangular 40x60" NGS WFS patrol field (yellow), the 40" field desired for the science instrument (blue) and a representative detector area (orange hatched).

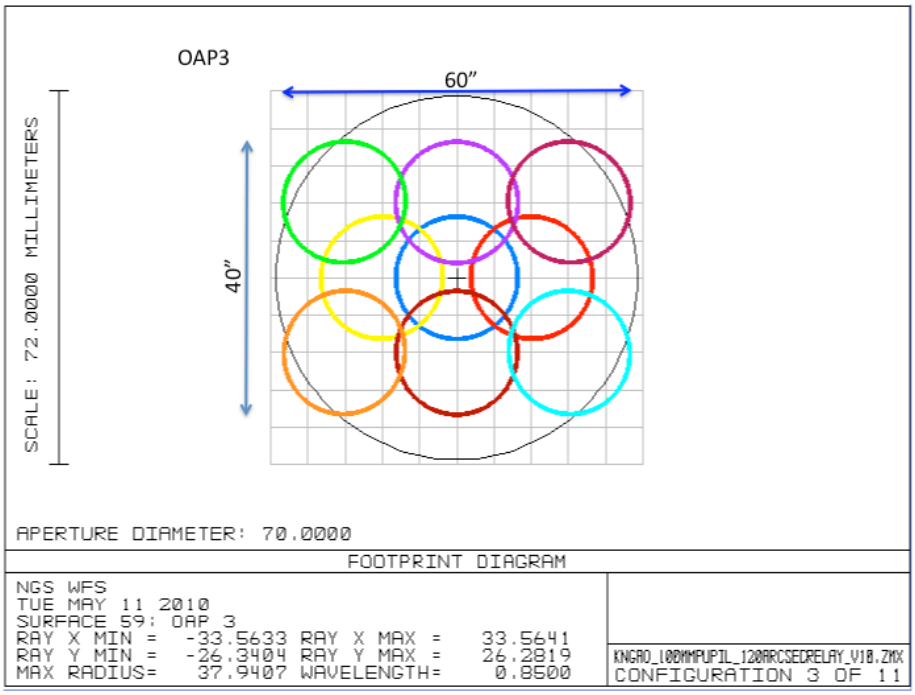

Figure 10. The first fold mirror of the second relay and OAP3 define the patrol field of the NGS WFS. The figure shows the footprint of the 40"x60" rectangular field of view accepted by the first fold of the second relay on OAP3.

3.9 Science Instrument ADC

A counter-rotating prism pair has been designed to compensate for the effects of atmospheric dispersion in the science instrument for the near-infrared wavelengths. Atmospheric dispersion will cause lateral separation of different wavelengths at the science image plane. The amount of displacement is a function of the wavelength and bandpass of the science observation, and the zenith distance of the observed object. It is therefore desirable to have a tunable ADC that can compensate at all wavelengths of interest, and all zenith distances.

We have based our design on NIRC2's NIR ADC, using the glass pairs of Silica and Calcium Fluoride for each of the prisms, and adjusting the prism angles to achieve the desired dispersion correction at the science path f/# and distance from focus. The prisms will be required to co-rotate to maintain alignment with the field. Figure 12 shows the NIR ADC at with prisms positioned to provide maximum dispersion.

When the ADC is inserted, the science focus will shift by 10.4 mm away from the ADC. The telescope will be refocused when the ADC is inserted to maintain the output focal plane at the science instrument detector. That will result in a shift of focus of 0.9 mm at the LOWFS pick-off, f/13.66 focal plane.

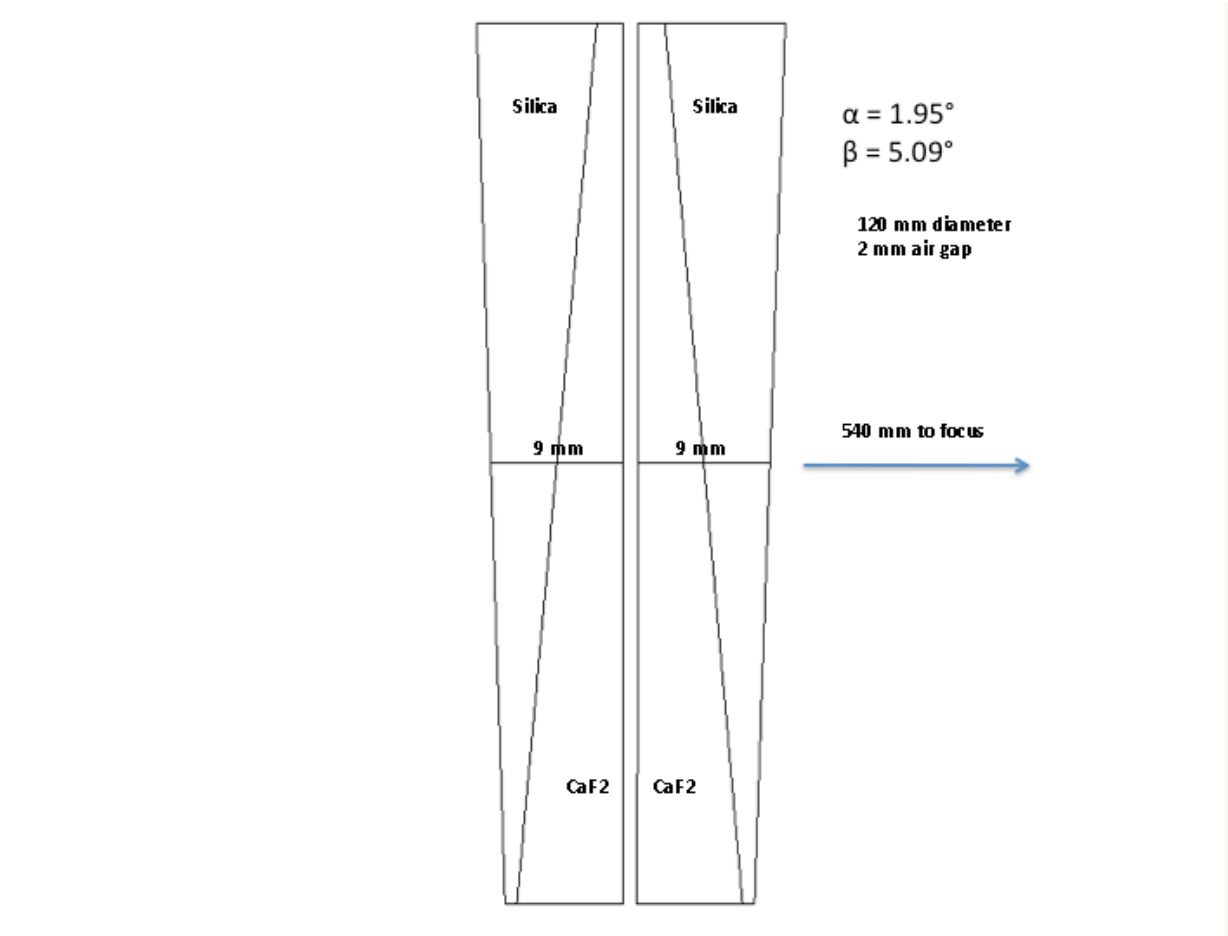

Figure 12. NGAO NIR ADC design.

The ADC described above corrects atmospheric dispersion down to wavelengths of 1 μ. For the visible wavelengths, a second ADC has been designed. It's located 302 mm ahead of the second relay focus. Like the NIR ADC, it consists of two counter-rotating prism pairs. The rotation mounts are placed on a linear stage for movement in and out of the beam.

4. Performance

To determine the performance of the optical system, several sources of optical degradation were analyzed using Zemax in the wavelength passbands used by the science instruments and wavefront sensors. The passbands are defined in KAON 530.

The optical relay was modeled in conjunction with the Keck primary and secondary mirrors, to ascertain the combined effects of the two optical systems.

Field points used were the maximum off-axis fields defined for each instrument. The wavefront errors and RMS spot radii quoted are the worst-case for the field points analyzed.

The working f/# of the wide-field relay is f/13.66 and of the narrow-field relay is f/46.3. Airy disk sizes are defined by

$$r_{airy} = 1.22\lambda F/\# \qquad (3)$$

and the depth of focus (DOF) is defined by $DOF = 4\lambda\left(F/\#\right)^2$.

Chromatic focal shift and lateral color, where applicable, were evaluated for different wavelength ranges using the Zemax analysis tools. Lateral color and chromatic focal shift arise in beam paths in which there are transmissive optics, such as windows and beamsplitters.

4.1 LOWFS

The matched OAPs used in the first relay give excellent performance over a wide field at infinite conjugate. The values given in Table 5 assume a flat low order DM and flat high order DMs in the individual LOWFS relays. The first relay gives diffraction-limited performance over the entire 120 arcsecond diameter field, as seen in Figure 14. Chromatic aberrations are due to the entrance window at the front of the AO relay.

Table 5. Performance of the LOWFS in simultaneous J and H bands.

Instrument (mode)	λ (μ)	F/#	FOV ″	Fld curv. (mm)	Sag due to fld curvatue (mm)	RMS WFE, on axis (nm)	RMS Spot Radius, on axis (mas)	RMS WFE, 60" radius (nm)	RMS Spot Radius, 60" radius, (mas)	Lateral color (μ)	Chrom. Focal shift (μ)	Depth of focus (mm)	Grid distortion, %
LOWFS	1.17-1.78	13.66	120	1200	0.9	9	3.5	42	7.2	0.5	180	0.9	1.5

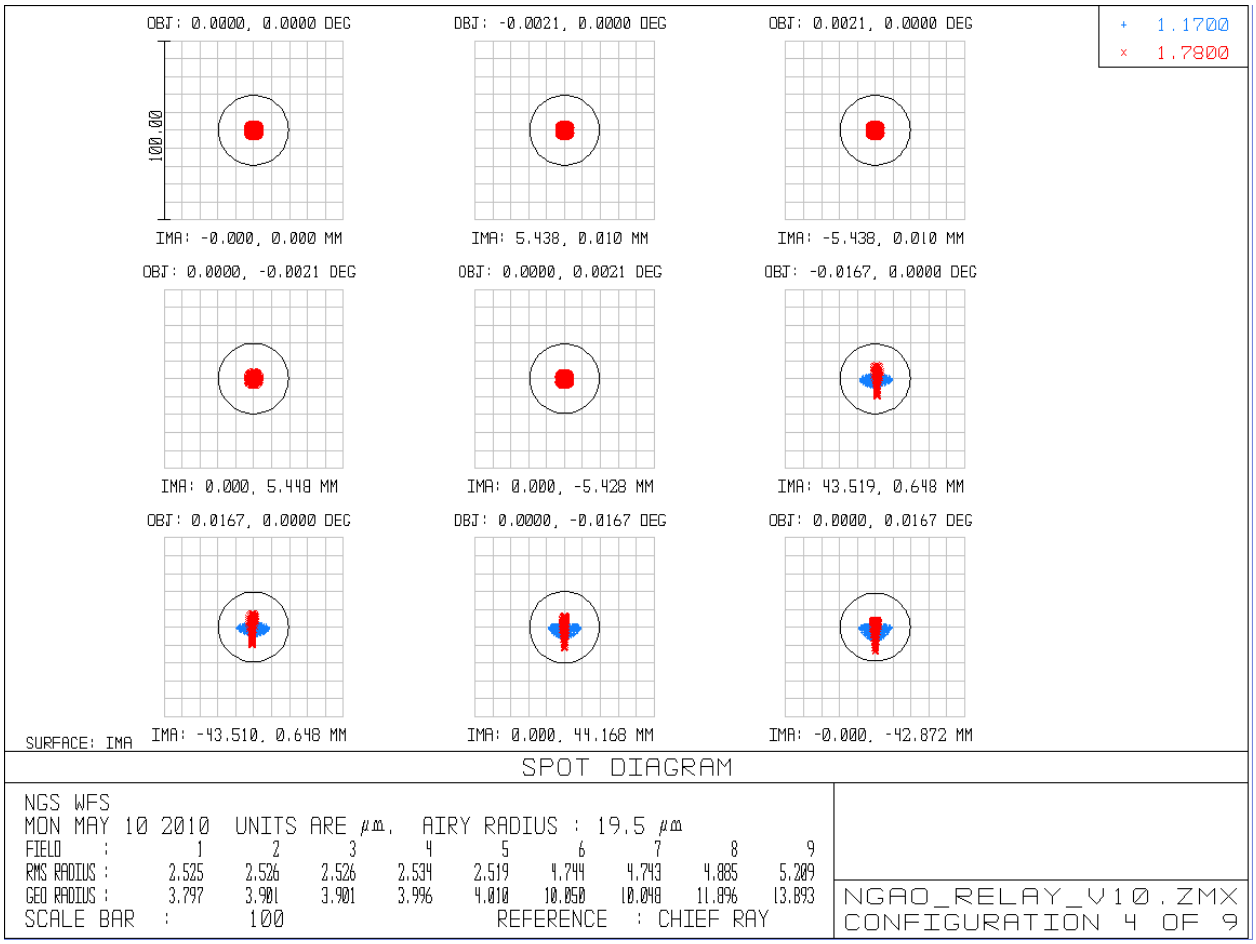

Figure 14. Spots at focal plane of f/13.66 LOWFS relay. The LOWFS will operate over the J and H-bands simultaneously, from 1.17-1.78 μ. Spots shown assume no DM correction. Scale circle is the diffraction limit at 1.17 μ.

4.2 Science Instruments, Narrow-field Relay

The second relay consists of two unmatched OAPs resulting in an increase of focal ratio to f/46.3. The larger focal ratio results in an image scale of 2.46mm/arcsecond at the focal plane. The second relay passes a 40" diameter field of view to the science instrument. The science instrument is intended to cover a wavelength range from i-band (0.7 μ) to K-band (2.4 μ).

The aberrations resulting from the non-matching pair of OAPs in the second relay are strongly field-dependent, so a correction applied to the high order DM does not result in better performance over the whole field. There is also a large amount of field curvature, which cannot be corrected by a DM at the pupil plane. The values presented in Table 4 include the effects of field curvature in the RMS WFE

Table 6. Performance of the narrow-field relay.

Observing band	λ (μ)	Fld curv. (mm)	RMS WFE (nm), on axis	RMS WFE (nm), 10" off axis	RMS WFE (nm), 20" off axis	RMS Spot Radius, on axis (mas)	RMS Spot Radius, 10" off axis (mas)	Airy radius (mas)	Chrom. Focal shift (mm)	Depth of focus (mm)
i-band	**0.7-0.85**	**220**	**29**	**18**	**70**	**10**	**10**	**14**	**1.5**	**6**
z-band	**0.85-1.05**	**220**	**29**	**18**	**70**	**10**	**10**	**17.5**	**1.5**	**7**
Y-band	**0.97-1.07**	**220**	**29**	**18**	**70**	**10**	**10**	**20**	**0.7**	**8**
J-band	**1.17-1.33**	**220**	**29**	**18**	**70**	**10**	**10**	**24**	**1**	**10**
H-band	**1.49-1.78**	**220**	**29**	**18**	**70**	**10**	**10**	**31**	**2**	**12**
K-band	**2.03-2.37**	**220**	**29**	**18**	**70**	**10**	**10**	**42**	**3**	**17**

Figure 15 shows the degradation of the optical performance with field angle. Figure 16 shows an example of the spots at the on-axis, mid, and extreme field angles of the science instrument. Because the dominant source of wavefront error is field curvature, the focus can be shifted to provide the best wavefront error on axis. In Figure 14 the focus has been adjusted to give the best performance over the central 20 arcsecond field of view.

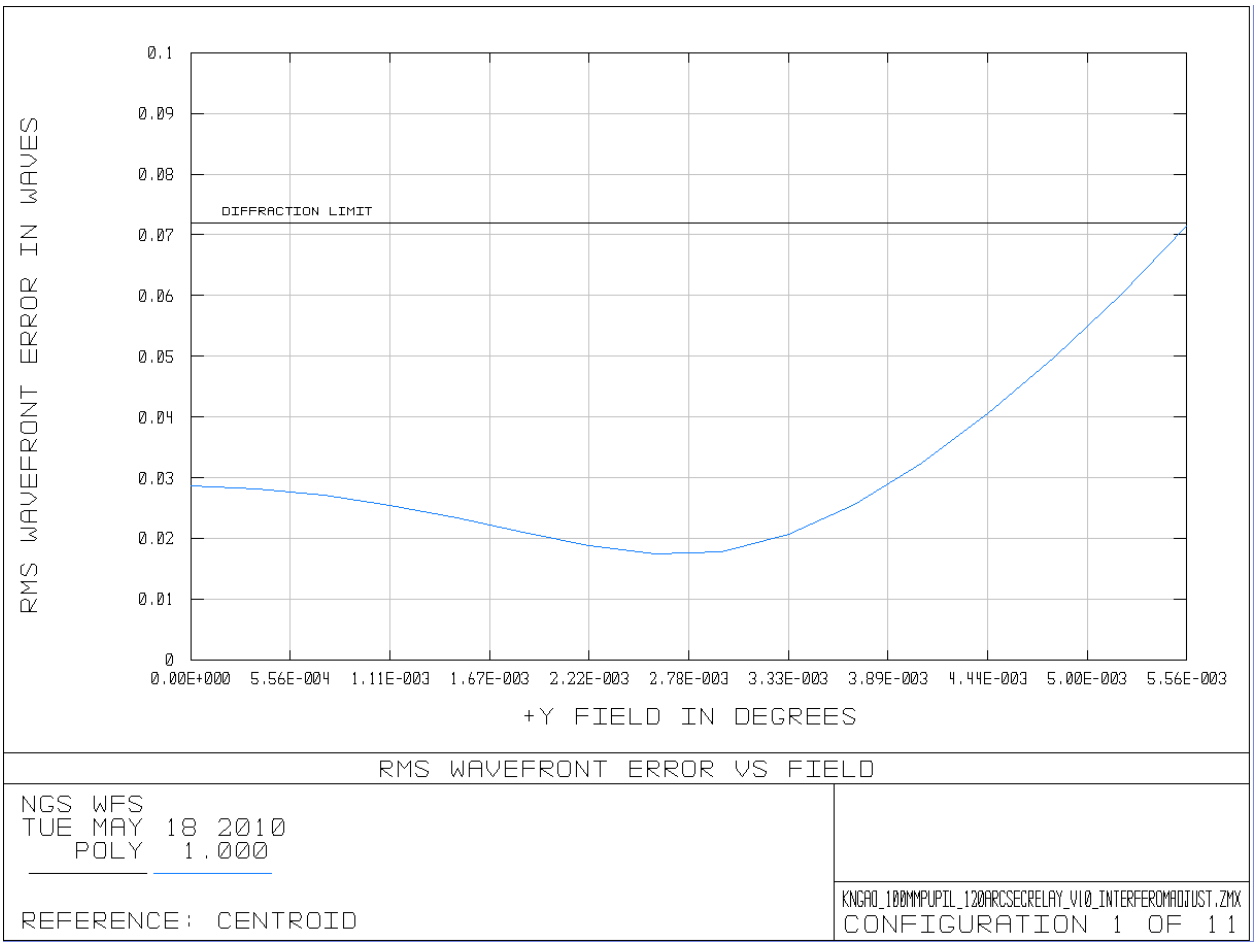

Figure 15. RMS wavefront error as a function of field. Field curvature is the dominant source of wavefront error. The focus has been adjusted to give the best performance over the central 20 arcsecond diameter field of view.

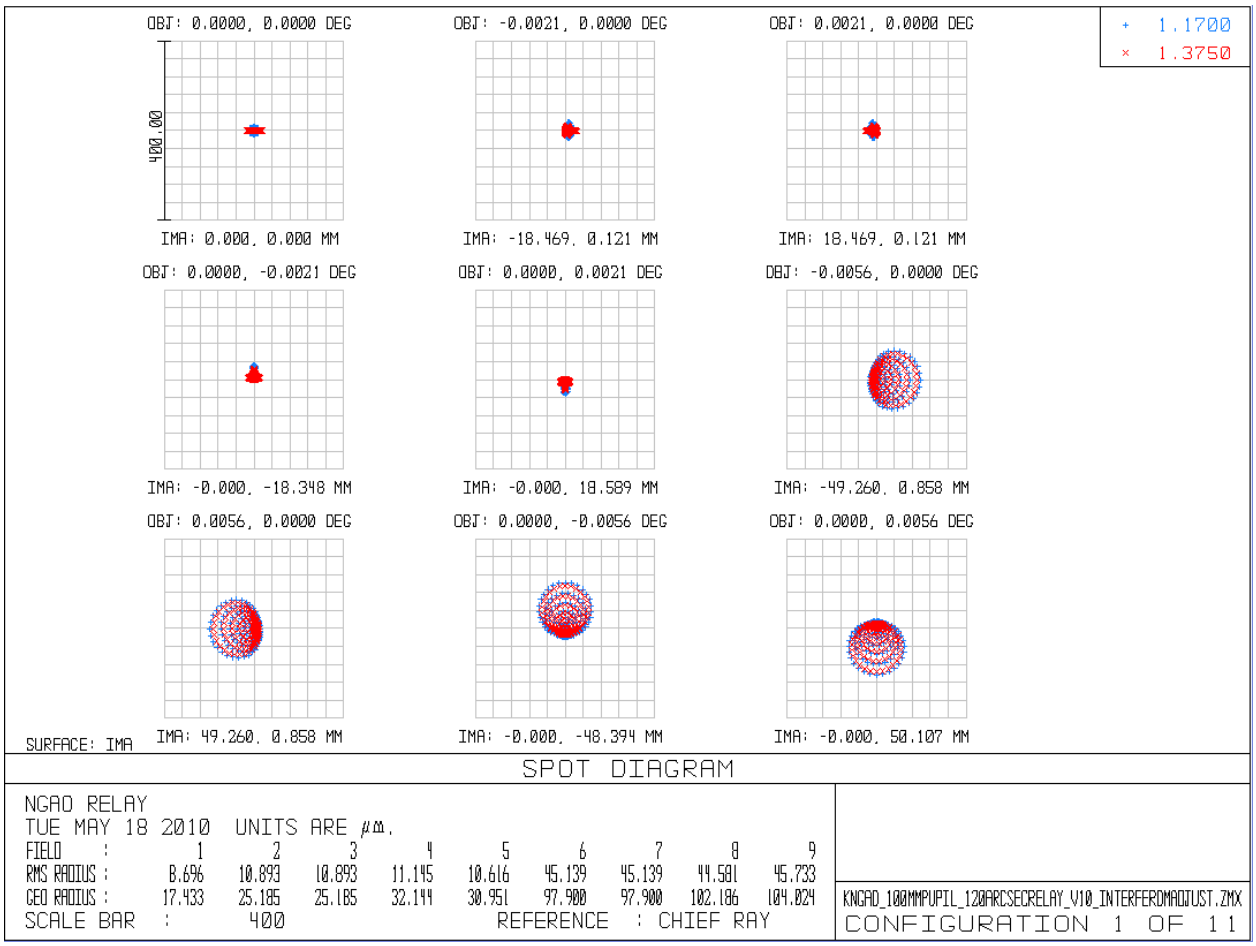

Figure 16. Spots in J-band at the focal plane of the science relay.

4.3 Laser Guide Star Wavefront Sensor (LGS WFS)

The LGS WFS dichroic pick-off lies in the space between the low order DM and OAP2. The laser guide stars, over a 120 arcsecond diameter patrol field, are re-imaged using a singlet biconvex lens with an aspheric surface. Because the relay passes only 589 nm sodium light, chromatic aberrations are not an issue. This lens was optimized for 90km (the spot size varies by only 10s of milliarcseconds between 90 and 180km). Table 5 details the performance of the LGS WFS relay. The tilt and curvature of the focal plane of the LGS WFS vary with the zenith distance of the guide stars. Figure 10 displays the RMS wavefront error as a function of field. Figure 11 shows spot diagrams on-axis and at extreme field positions for a zenith angle of 39°.

Table 7. Performance of LGS WFS

Conjugate height	FOV, arcsec	Focal plane tilt °	Field Curvature (mm)	Grid distortion	RMS WFE, on axis (nm)	RMS WFE, at 60" radius (μ)	RMS Spot Radius, on axis (mas)	RMS Spot Radius , 60" radisus, (mas)
90 km	120	4	4000	0.7%	140	1.8	33	253
115 km	120	3	9500	0.7%	140	1.9	33	285
180 km	120	2	>10,000	0.8%	140	2.2	33	323

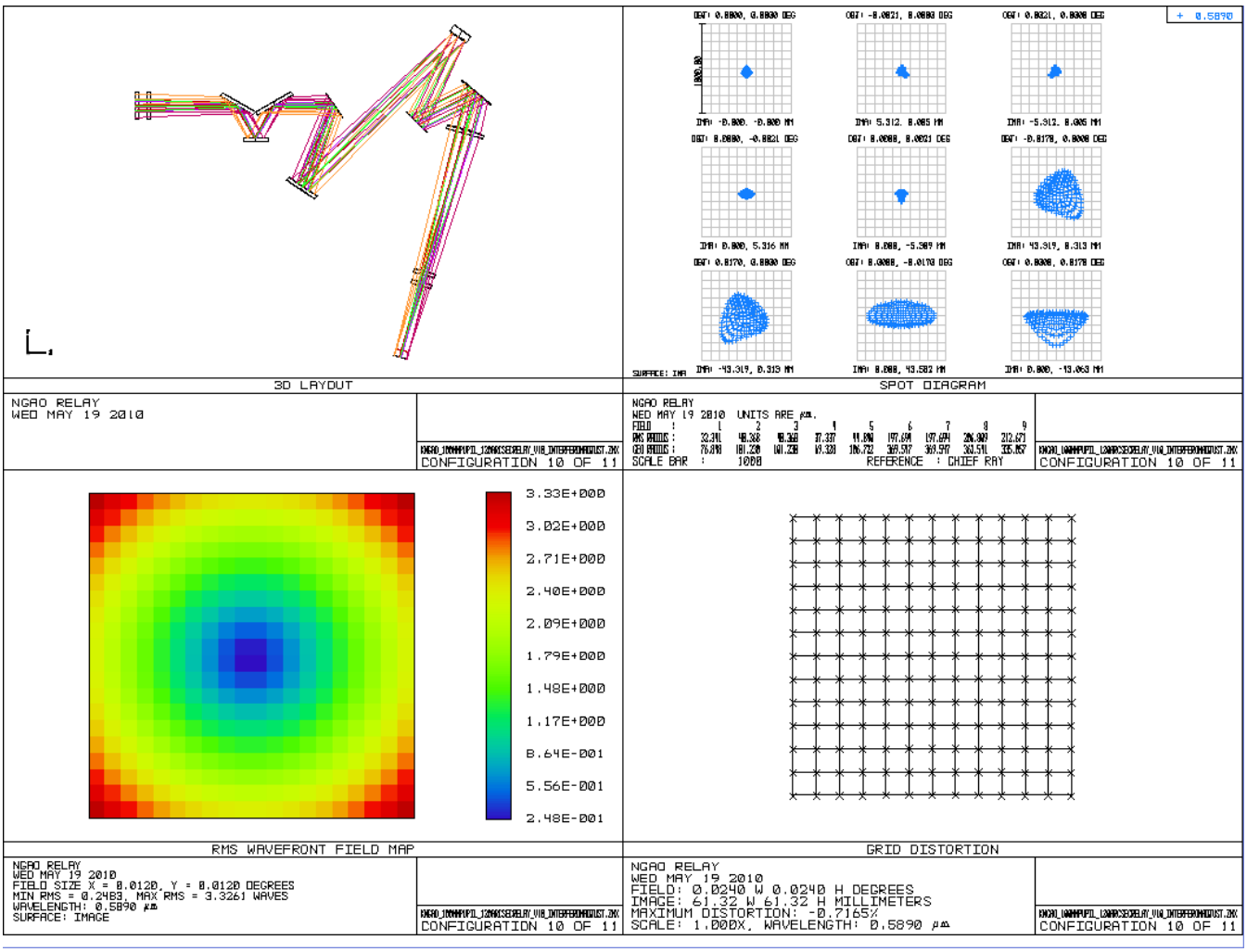

Figure 18. Performance of the LGS WFS relay at an object distance of 115 km (about 39° zenith angle). Top right: full-field spot diagram over the entire 120 arcsecond patrol field. Bottom left: RMS wavefront error as a function of field position. Bottom right: distortion map over field.

To determine whether this amount of laser guide star wavefront aberration is acceptable requires further analysis. As seen in Figure 18, the spot size of the laser guide stars produced by the OAP/bi-convex relay is roughly 300 milli-arcseconds at the edges of the 120 arcsecond diameter field. According to KAON 551, WFS sub-system conceptual study report, this compares to other factors as follows: diameter of point source laser at Na layer, 1.08 arcseconds; seeing, 470 milli arcseconds; elongation, 850 milli-arcseconds; diffraction limit of subaperture, 660 milli-arcseconds. The relay static aberration contribution to spot size is smaller than all of these, and is much smaller than the combined 1.47 arcsecond expected laser guide star size. The error budget shown in KAON 551, Table 2, allows a 250 milliarcsecond spot size ”due to aberrations in AO thru to WFS”. It’s not clear whether this includes contributions from the WFS optics. This requirement needs clarification..

Another concern is the effect of the wavefront error on the dynamic range of the Shack-Hartmann wavefront sensors. The static aberration will cause movement of the Hartmann spots from the centers of the subapertures. If the static aberrations cause the Hartmann spots to move a significant fraction of a subaperture, that subaperture will be compromised in its dynamic range. To evaluate the extent of this problem, the position of the Hartmann spots in the subaperture, due to static aberrations, were evaluated in three ways: through Zemax modeling of the LGS WFS, a simplified analytic approach, and through computer modeling of the Hartmann sensor.

In Zemax the wavefront sensors were modeled using non-sequential components. Each field point encountered its own collimating lens, which imaged the telescope pupil onto a lenslet array. The resulting Hartmann pattern allowed visual inspection of the placement of the Hartmann dots, given the static aberrations at each field point. Figure 19 shows no gross Hartmann spot displacements on an 18x18 subaperture grid. The 64x64 subaperture grid specified for NGAO is difficult to model in Zemax, due to computation time.

Figure 20 shows an approximate calculation of the spot displacements given the wavefront errors in the extreme field points. The static aberrations consist mostly of astigmatism, and analysis in Zemax indicates about 9 microns peak-to-valley of astigmatism is present in the extreme field positions. This corresponds to Hartmann spot displacements of approximately 6% of the subaperture.

Finally, a Hartmann sensor simulator developed by Mark Ammons and Don Gavel of the LAO was used to assess the spot movement. Again, the static aberrations were assumed to be astigmatism with an approximate magnitude of 9 microns peak-to-valley. This wavefront phase error, modeled as a Zernike polynomial with coefficients corresponding to pure astigmatism, was propagated through a 64x64 subaperture lenslet array, and the resulting centroid shifts were measured. The model assumes Fresnel propagation to the lenslet array focus. Figure 14 shows an example of one pupil edge of the Hartmann sensor, with the subaperture boundaries drawn in and the shift of the Hartmann spots due to astigmatism visible. The center of mass centroiding results shown in Figure 15 predict shifts of approximately 5-6% of a subaperture, consistent with our analytic calculations in Figure 13.

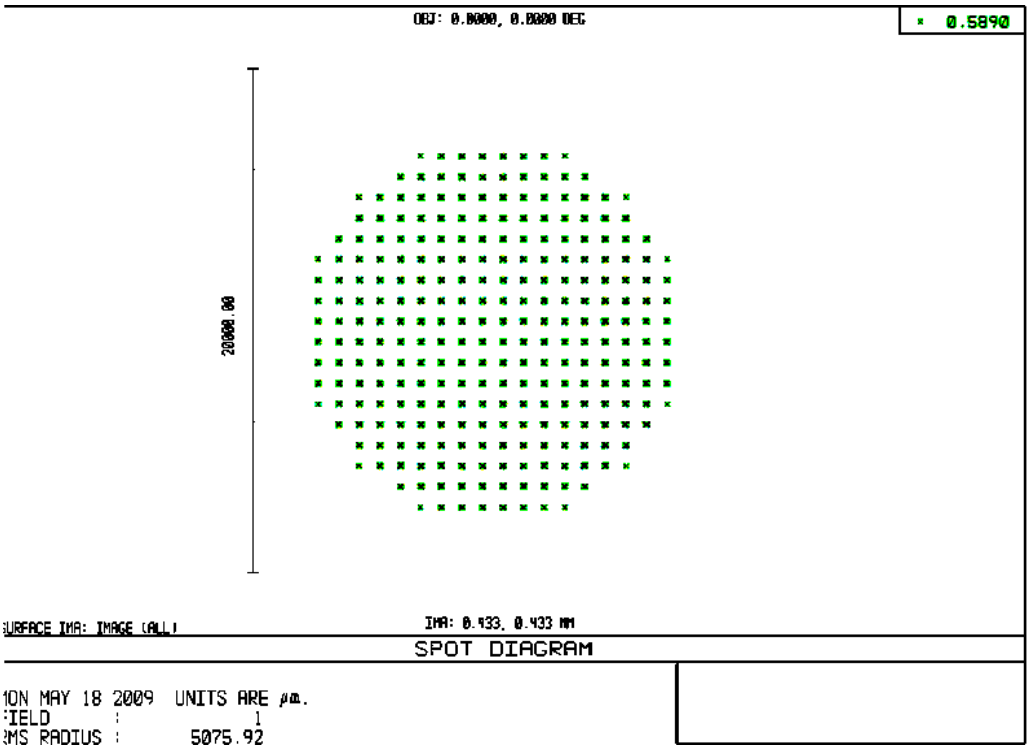
OBJ: 0.0000, 0.0000 DEG
0.5890
20000.00
URFACE IMA: IMAGE (ALL)
IMA: 0.433, 0.433 MM
SPOT DIAGRAM
ION MAY 18 2009 UNITS ARE μm.
IELD : 1
MS RADIUS : 5075.92

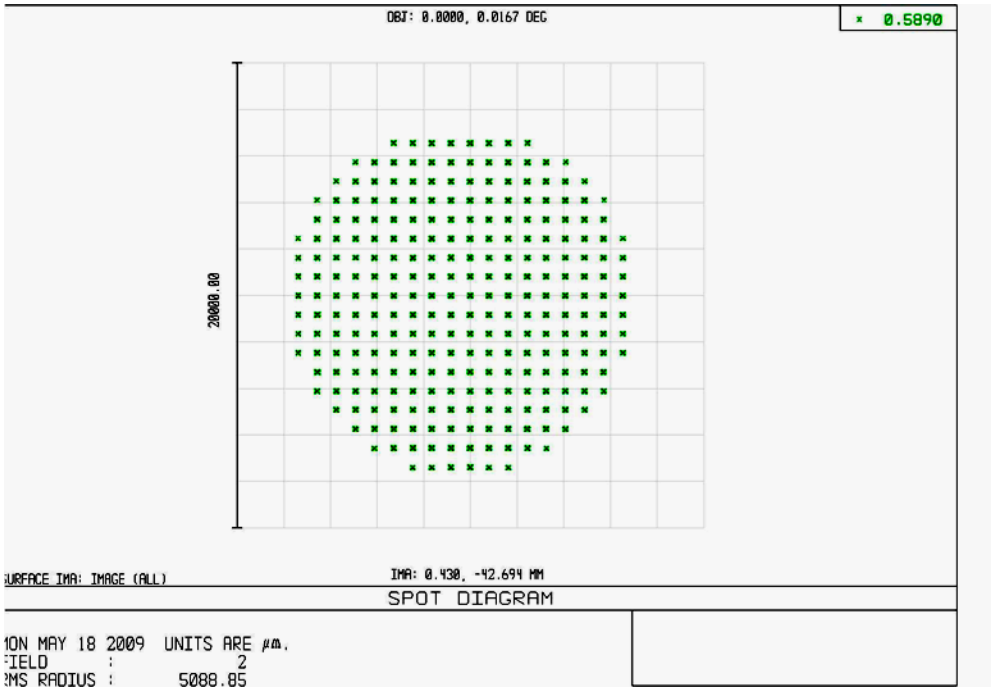
OBJ: 0.0000, 0.0167 DEG
0.5890
20000.00
URFACE IMA: IMAGE (ALL)
IMA: 0.430, -42.694 MM
SPOT DIAGRAM
ION MAY 18 2009 UNITS ARE μm.
IELD : 2
MS RADIUS : 5088.85

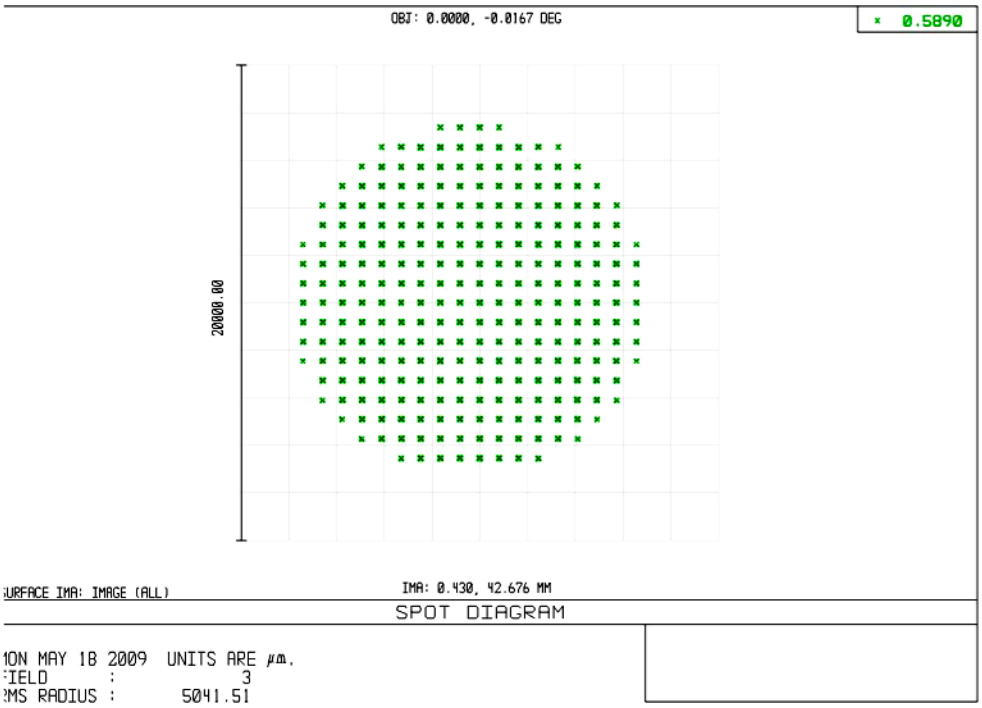

Figure 19. Zemax modeling of the on-axis (top) and extreme x and y field positions (120" diameter field of view) LGS WFS. For each field position, a separate f=180mm collimator lens imaged a pupil on an 18x18 subaperture lenslet arrays. The spot diagrams show the Hartmann spots produced by each of the lenslet arrays. Visual inspection shows no pronounced displacement of spots due to static aberrations in the LGS relay. An 18x18 subaperture lenslet array was assumed for ease of display and speed of computation.

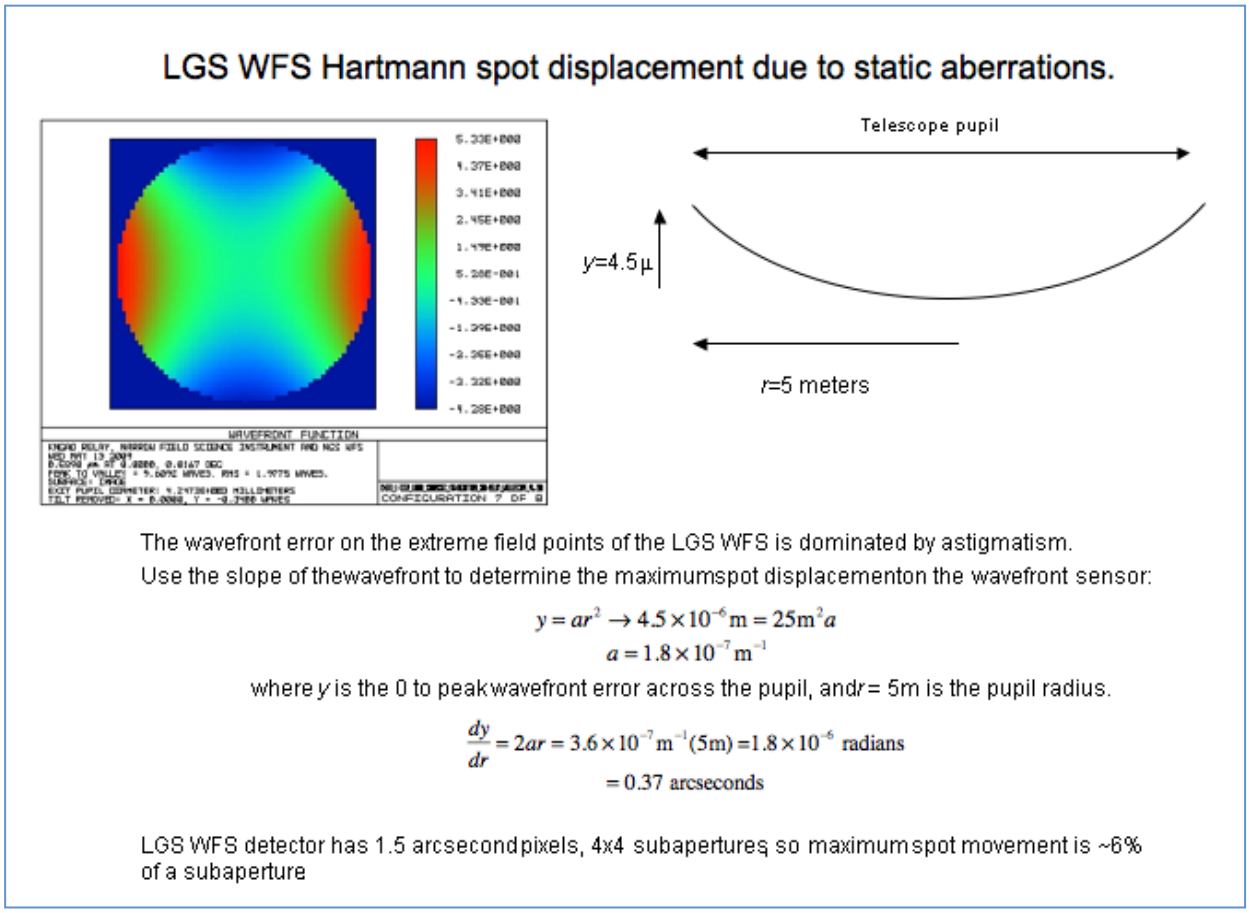

Figure 20. Simple analytical treatment of Hartmann spot displacement due to static aberrations in LGS WFS optical path. The static aberrations at the extreme field points are dominated by astigmatism, as shown in the false color wavefront in the upper left. This will cause a Hartmann spot displacement of roughly 6% of a subaperture at the edges of the pupil.

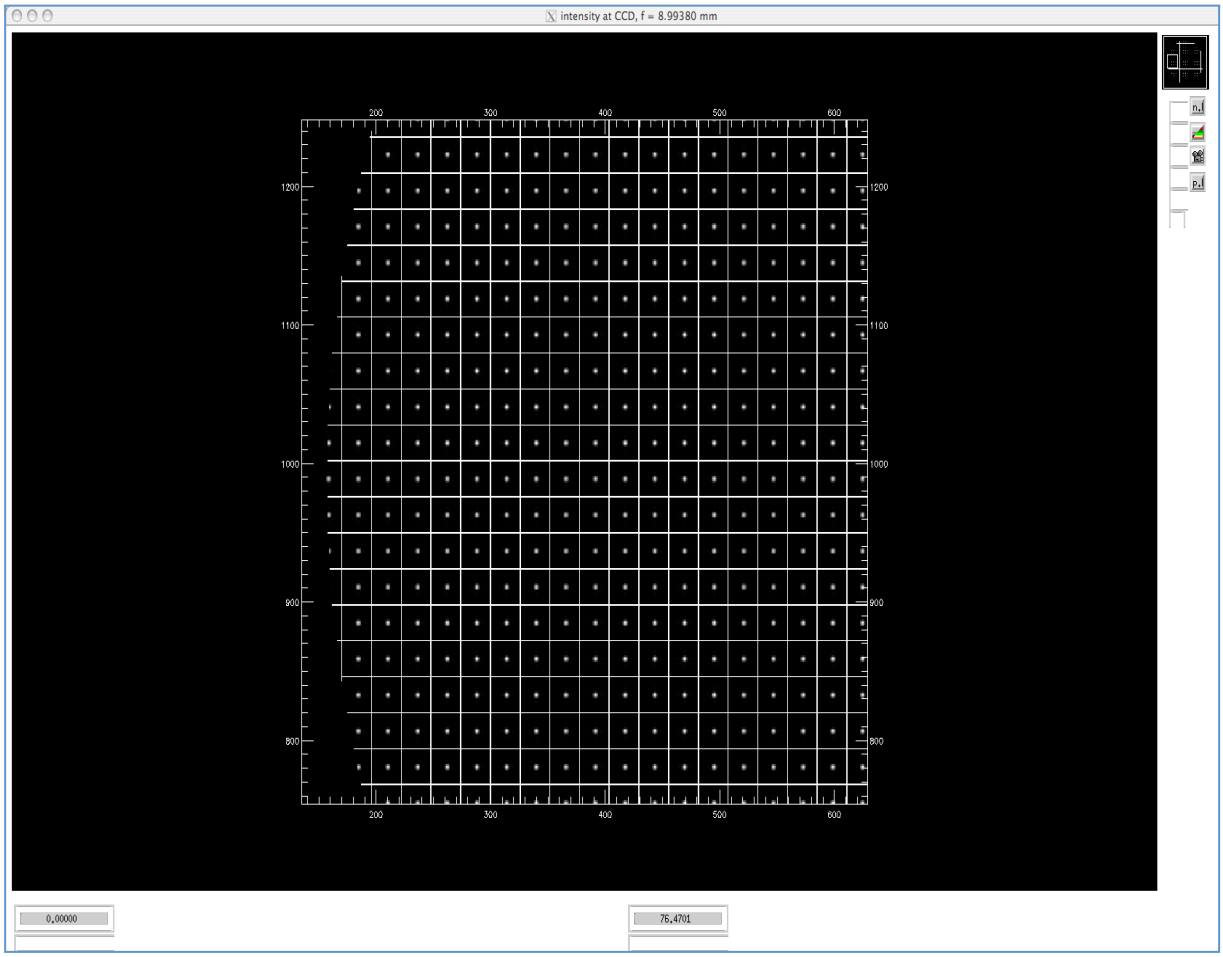

Figure 21. Results of a Hartmann sensor simulation given the static errors present in an extreme field position of the laser guide star wavefront sensor relay. At 60 arcseconds radius, the wavefront entering the wavefront sensor optics is expected to have as much as 9 microns peak-to-valley of predominantly astigmatism. This extreme static aberration is due to the optical relay's optimization for objects located at infinity (natural stars), while the laser guide star varies between 90 and 180 km above the telescope. The image above shows the location of Hartmann spots with respect to the subaperture grid, at one edge of the pupil.

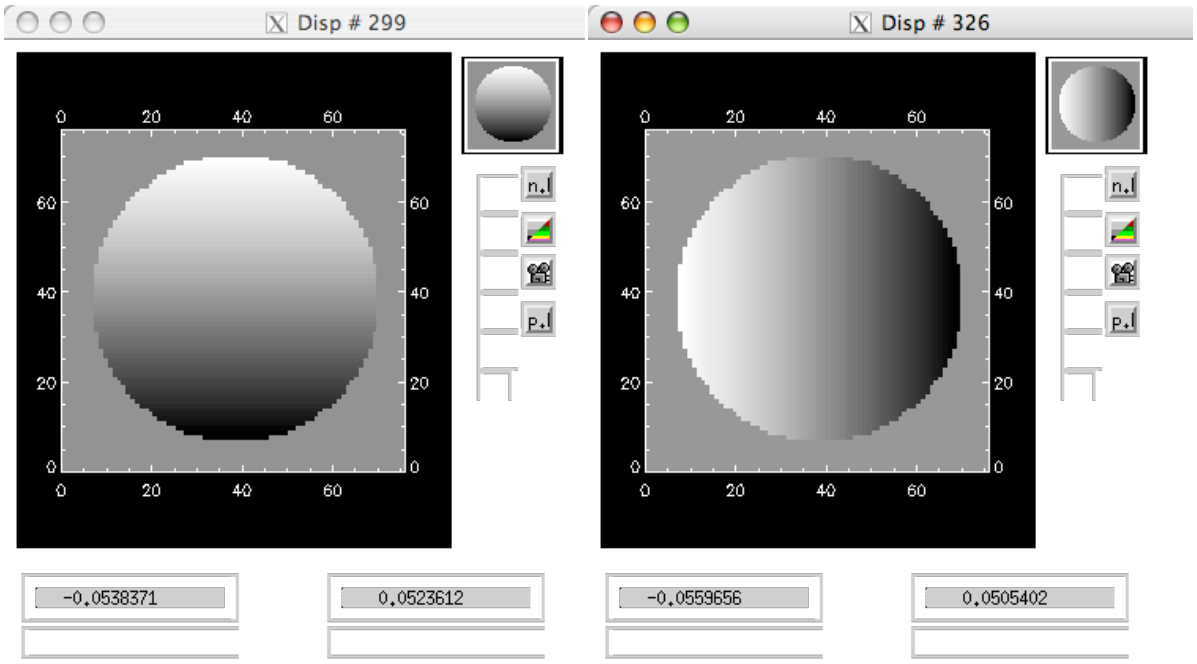

Figure 22. Given the Hartmann spot locations shown in Figure 21 over the entire pupil, centroids were calculated and are displayed above, normalized to the subaperture width. X centroids (left) and Y-centroids (right) are displaced by static aberrations by approximately +/- 5% of a subaperture at the edges of the pupil.

4.4 Pupil Distortion on Deformable Mirrors

We have included drawings of the mapping of the Keck telescope primary mirror on the low order (Figure 18) and high order (Figure 19) deformable mirrors. The mapping includes the 10 degree incidence angle on both the mirrors. The low order mirror in Figure 18 is the Gemini DM4.5 designed by CILAS. It's 22x22 actuators are on a 5mm pitch. The high orde mirror in Figure 18 is the 64x64 MEMs device designed for the Gemini Planet Imager project. Its actuators are on 0.4mm centers.

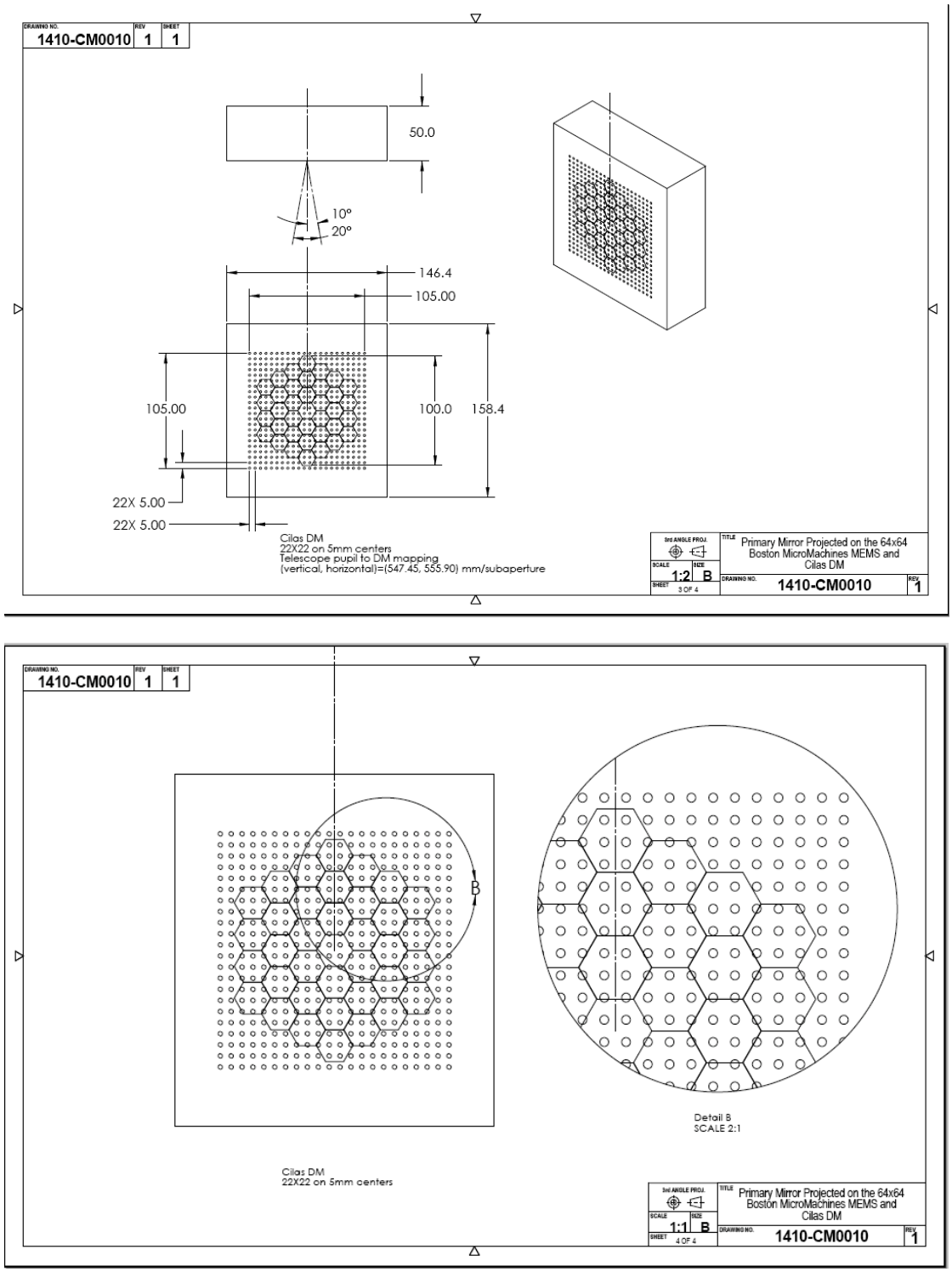

Figure 18. The telescope pupil mapped on the low order deformable mirror. The DM used in this drawing is the 22x22 actuator, 5mm pitch device designed for Gemini. Figure courtesy of Jim Bell. (See document 1410-CM0010)

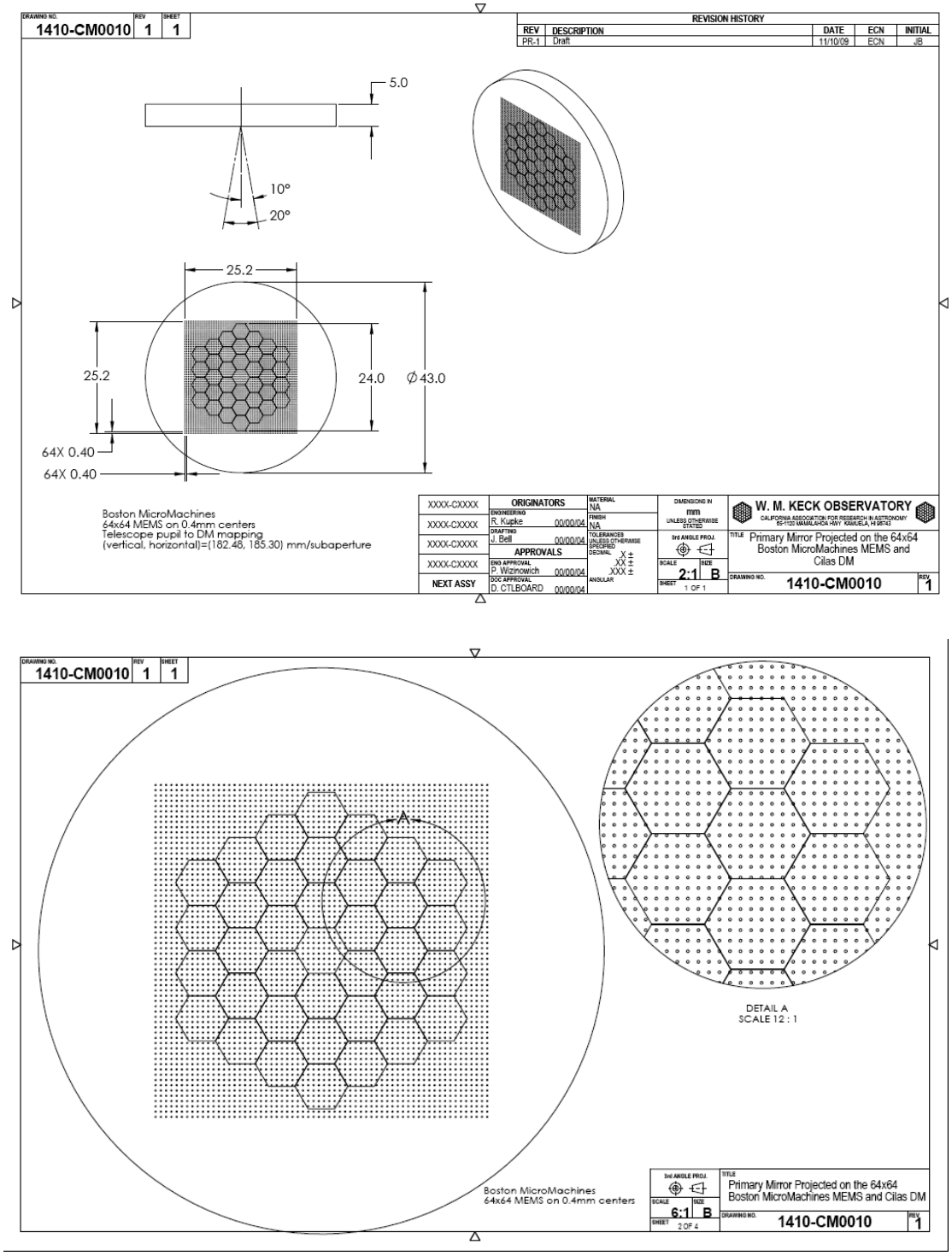

Figure 19. The telescope pupil mapped on the high order DM. The pupil image is 24mm in diameter, covering 60x60 actuators of the 64x64, 0.4mm pitch device. Figure courtesy of Jim Bell. (See document 1410-CM0010)

Pupil distortion in the NGAO relay manifests itself in at least three ways. The first is the degree to which a grid of points on the primary mirror maps to a demagnified, but square grid on the

DM. Another consideration is the field-dependent pupil aberrations. This effect causes the chief rays from the various field angles to not all pass through the center of the pupil (paraxially, the chief rays all pass through the center of the pupil, by definition, but for real rays, this is not generally true). In other words, the pupil (i.e., the DM and the correction it applies to the wavefront) is shifted with respect to the telescope primary by an amount depending on the field angle—this is similar to anisoplanatism caused by atmospheric aberrations at an altitude not conjugate to the DM. Finally, a third effect is DM-to-lenslet misregistration and scale errors. This depends on the pupil re-imaging optics chosen for the wavefront sensors.

In the analysis, the telescope primary became the "object", and field points were defined on the edges of the primary mirror. Observed field angle was set by adjusting the "stop" size placed at the Nasmyth focus to accommodate a 120 arcsecond diameter field for the low order, and a 40 arcsecond diameter field for the high order DM in the narrow-field relay. Results are shown in **Error! Reference source not found.** and following figures. Requirement FR-1505 specifies that the first relay shall have no more than 0.5% grid distortion at the pupil. As seen in Figure 25 , the first relay exhibits 0.43% grid distortion at the low order DM. Requirement FR1506 specifies that the second relay have no more than 0.2% grid distortion. Unfortunately, the relay design does not meet his requirement, as Figure 26 shows, having a grid distortion of 0.26% at the MEMs DM. FR-1507 and FR-1508 require that the pupil aberrations be no more than a tenth of a subaperture in the first and second relays, respectively. The first relay meets this requirement. As seen in Figure 27, the image of the pupil on the deformable mirror produces 0.24mm FWHM spots when considering a 120" field. This is 5% of a subaperture. The second relay, however, does not meet the 10% requirement. It produces 0.06mm spots on the 0.4mm subaperture, or 15% of a subaperture when the science field of 40" is considered.

Error! Reference source not found. also summarizes the pupil tilt and curvature on the low order and high order DMs. FR-1510 and FR-1511 specify that the pupil tilt will be no more than 1 km on sky for the high order DM and 250m on sky for the low order DM. We are well within these requirements.

Table 8. Characteristics of the pupil image on the deformable mirrors

	Diameter (mm)	Field (″)	# actuators	Tilt (meters on sky, peak)	Curvature (mm)	Max Grid Distortion	Pupil PSF, (μ)
DM1, high order DM	100	120	20x20	134	3000	0.4%	400
DM2, low order DM	24	40	60x60	366	275	0.5%	81

4.5 Transmission

Transmission estimates were made in support of NGAO Performance flowdown budgets and can be found in KAON 723. Table in Appendix lists the substrates and coatings of each of the optics in the AO relay.

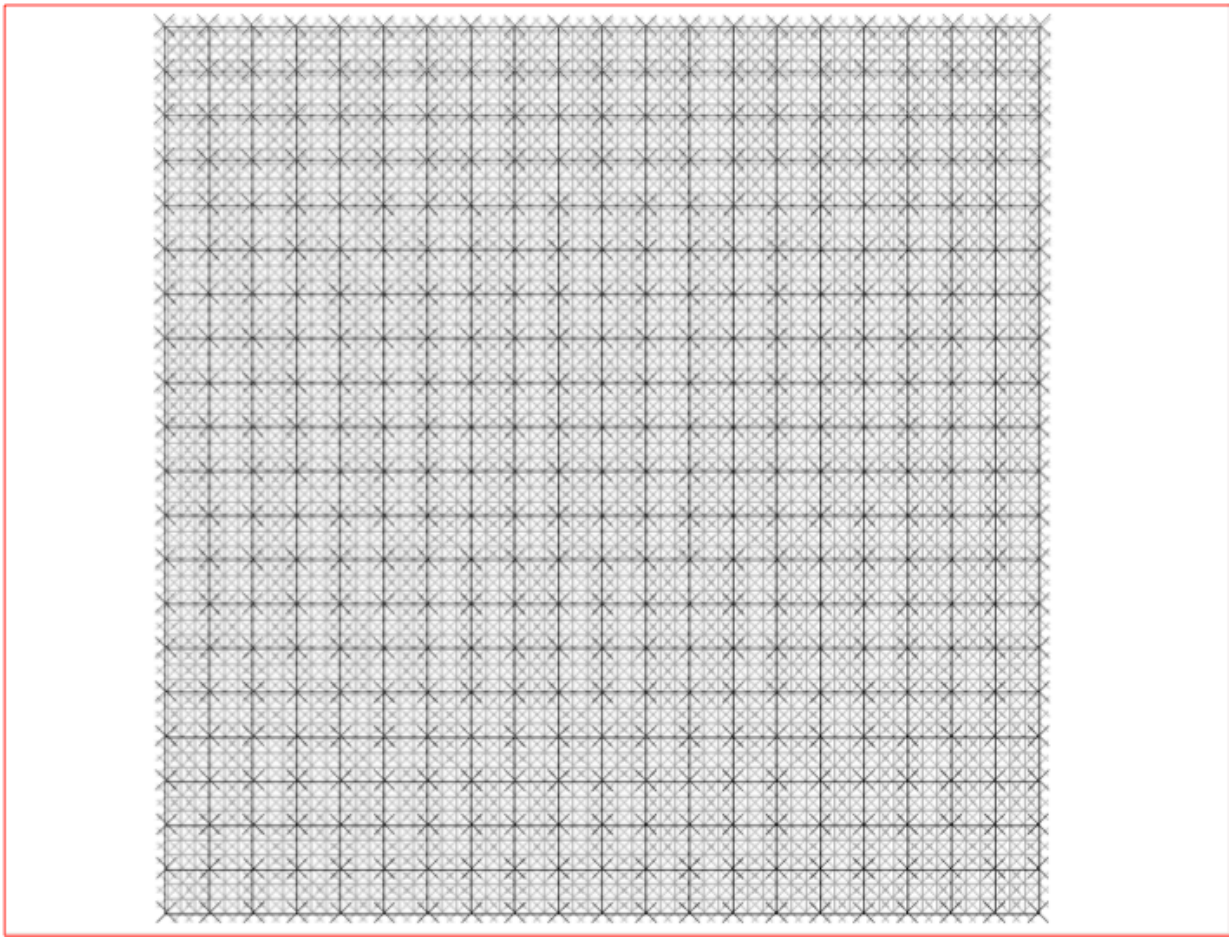

Figure 25. Mapping of the low order DM actuators (dark x's, 20x20) onto the high order DM actuators (fainter x's, 60x60). The grid lines represent the telescope primary, or perfect pupil image. Because the grid distortion is low for pupil imaging, the high order DMs map three actuators per one actuator low order DM out to the edge of the pupil.

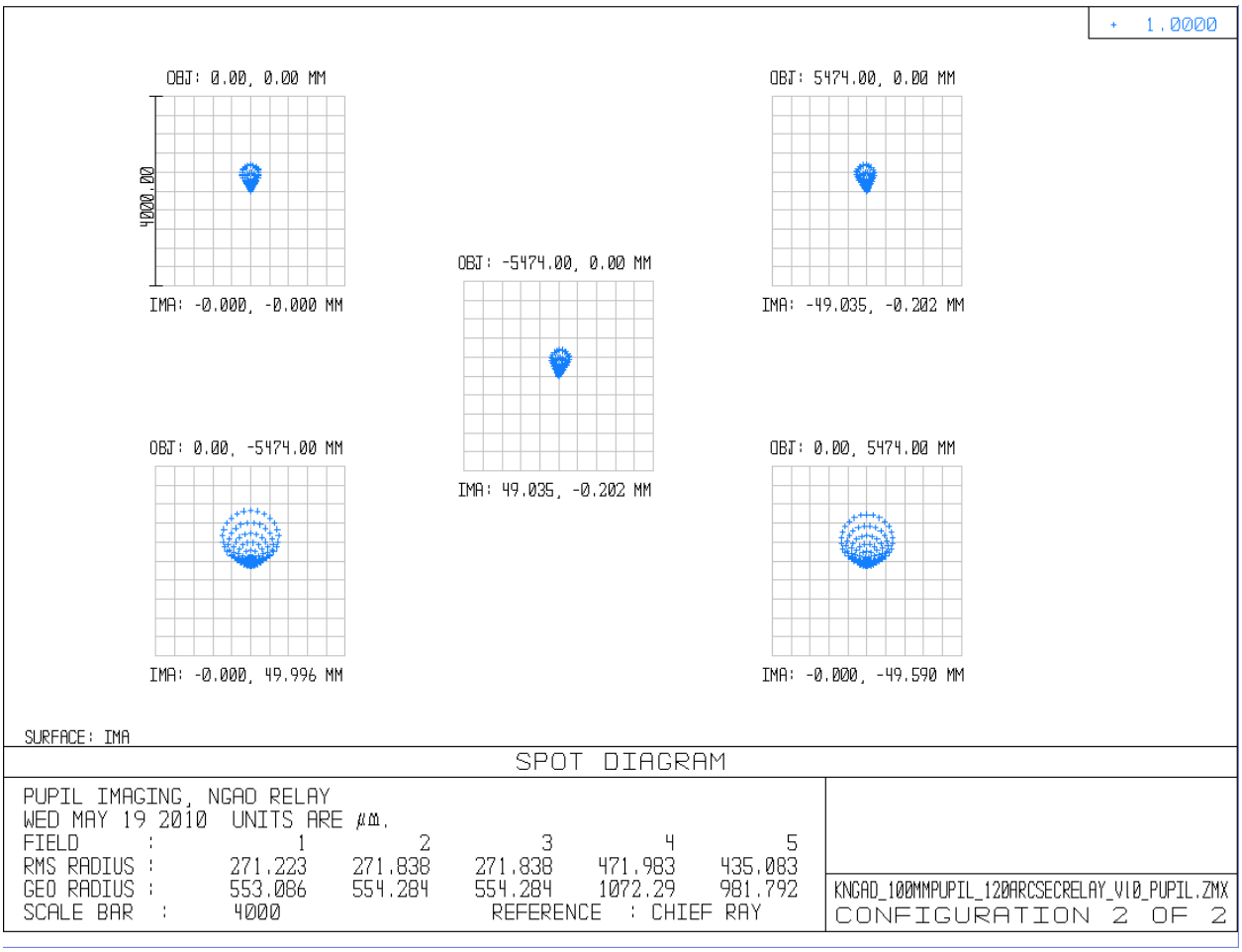

Figure 26. Geometric spot analysis of primary mirror imaged onto low order DM. Pupil tilt and curvature are included.

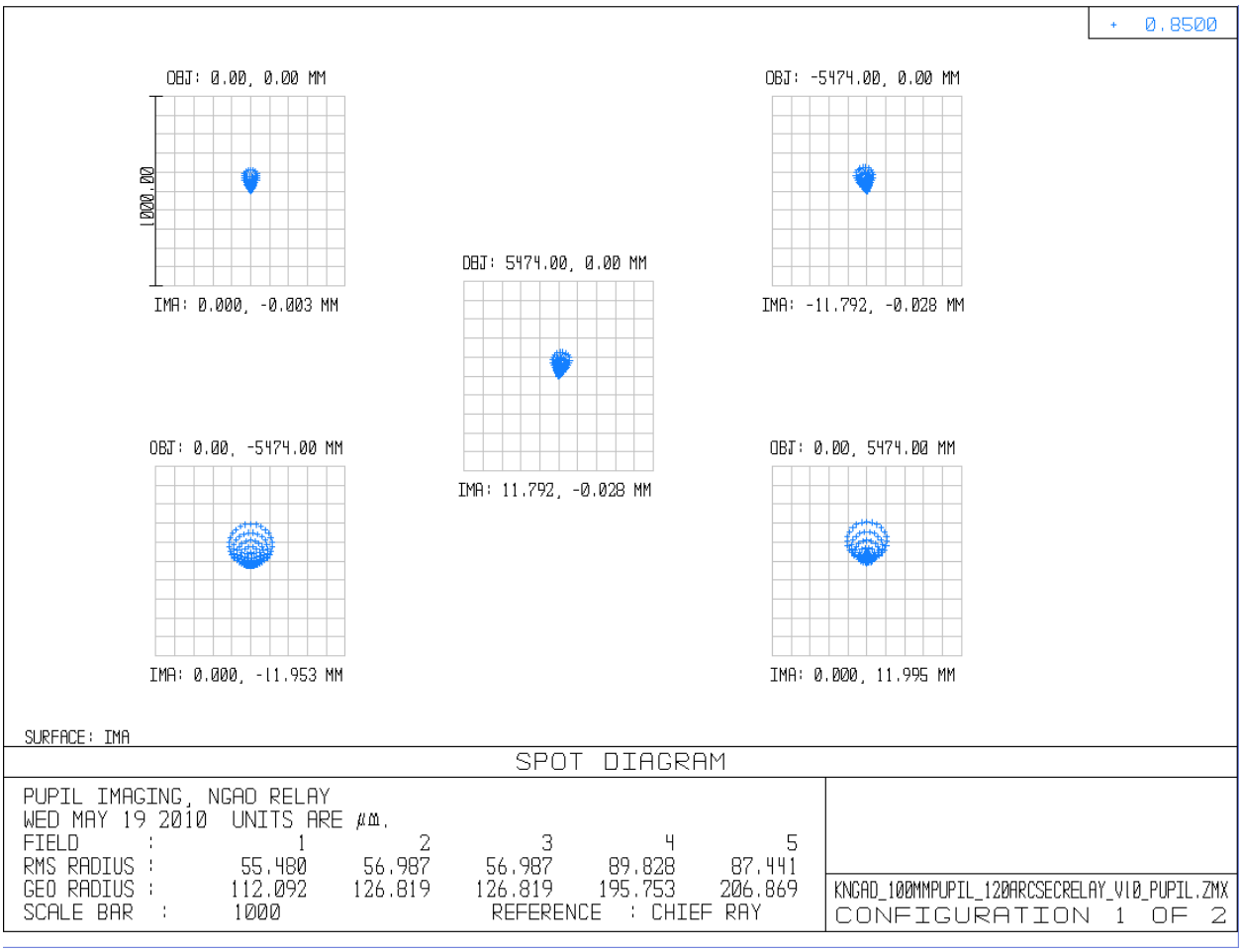

Figure 27. Geometric spot analysis of primary mirror imaged onto high order DM. Pupil tilt and curvature are included.

4.6 Telecentricity

Three of the outputs of the relay require the exit pupil of the relay to be located at infinity. The Zemax EXPP (exit pupil position) operand unfortunately is not valid for decentered systems (Zemax manual, June, 2007, p442). To roughly check telecentricity a paraxial lens with a focal length of 200mm was added to the focal plane of each relay. A pupil at infinity will image at exactly 200mm from the paraxial lens. Figure 29, Figure 30, and Figure 31 show the re-imaged pupil planes of the LGS WFS relay, the LOWFS (first) relay, and the science (second) relay, respectively. The image of the pupil is the location where all the field points cross. In this way large deviations from telecentricity can be discovered.

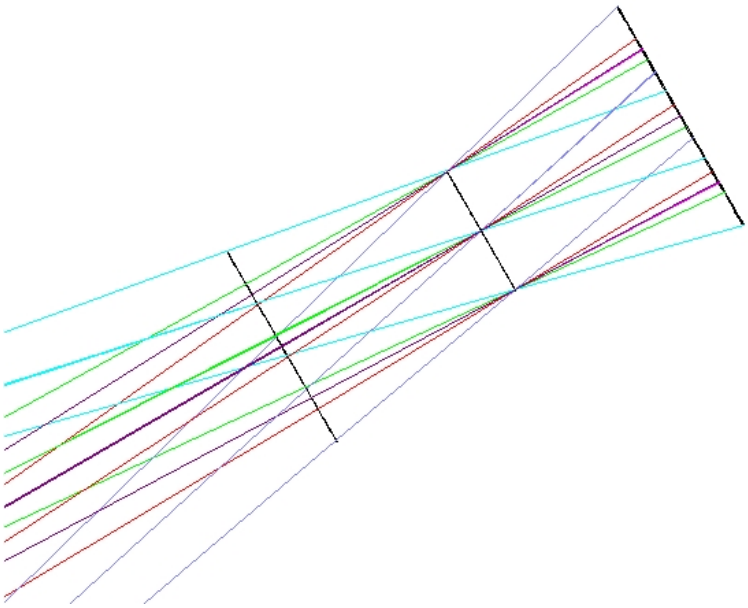

Figure 29. A paraxial lens has been placed at the focus of the LGS WFS relay. It produces a pupil image one focal length away (center line). For scale surfaces are placed 25mm before and after the focal length of the paraxial lens.

Figure 30. A paraxial lens has been placed at the focus of the LOWFS relay. It produces a pupil image one focal length away (center line). For scale surfaces are placed 25mm before and after the focal length

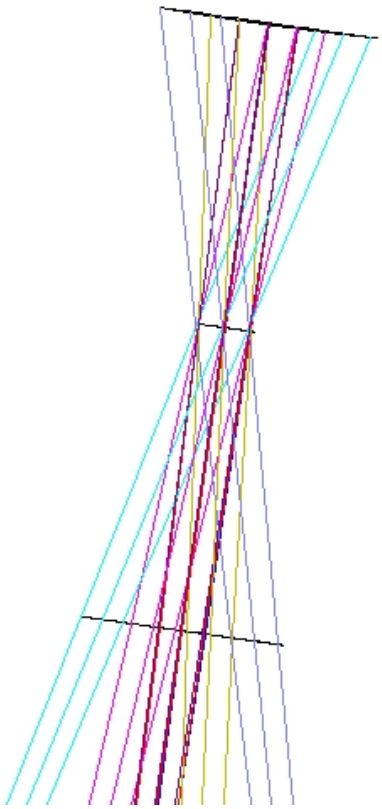

Figure 31. A paraxial lens has been placed at the focus of the science relay. It produces a pupil image one focal length away (center line). For scale surfaces are placed 25mm before and after the focal length

5. Optical Tolerancing

5.1 OAP off axis angle and focal length

The tolerance analysis was carried out both analytically and within Zemax. The OAPs, in particular, were subjected to an analytical tolerance analysis similar to that performed in KAON 107, "Science Path Optical Design" to evaluate the effect of errors in both the focal length and off-axis angle on the DM position, pupil size, and exit pupil position.

Tolerancing work derived from KAON 107.

5.1.1 Focal length tolerance

Impact of an error in radius of curvature or focal length, $f=f+\delta f=f(1 + \delta f/f)$.

A. Identical errors for both OAPs

Consider the case of an identical error for both OAPs of the first relay. The first-order solution to minimizing the impact is to move the components to compensate for this error.

1. The first OAP will need to be located a distance δf farther from the telescope focal plane.
2. The collimated beam diameter will be increased by $d_{DM}'/d_{DM}=1 + \delta f/f$.
3. The DM will be moved to be conjugate to the new pupil location. The distance to the DM from OAP1 becomes:

$$t_{OAP1,DM'} = \left[\frac{1}{f+\delta f} - \frac{1}{t+(f+\delta f)}\right]^{-1}$$

   where t is the distance from the focal plane of the telescope to the exit pupil.

4. The second OAP will be moved to provide a telecentric beam to the LOWFS image plane. This new location will be $t_{DM',OAP2} = f + \delta f$.
5. The output focal ratio will not change.

B. Error on OAP1 only

If only one OAP has a error, δf, in focal length, then steps 1-3 above still apply.

4. The second OAP will be at a distance f from the DM.
5. The ratio of the output focal ratio to the input focal ratio will be

$$f/\#_{out} \Big/ f/\#_{in} = \frac{\frac{f}{d_{DM'}}}{\left[\frac{f+\delta f}{d_{DM'}}\right]} = \left(1+\frac{\delta f}{f}\right)^{-1}.$$

6. The DM, second OAP and science instrument do not move significantly.

C. Error on OAP2 only

If the first OAP is perfect, and OAP2 has an error in focal length of δf, then steps 1-3 of case A are not required since there is no change in the position of the collimated beam diameter or the separation of the DM from the first OAP. We can start at step 4 of case A:

4. The second OAP will be moved to provide a telecentric output, $t_{DM',OAP2} = f + \delta f$.

5. The ratio of the output focal ratio to the input focal ratio will be the reciprocal of case B, step 5, or

$$f/\#_{out} \Big/ f/\#_{in} = \left[\frac{f+\delta f}{d_{DM'}}\right] \Big/ \frac{f}{d_{DM'}} = \left(1+\frac{\delta f}{f}\right)$$

Summary: The above equations are used in the following tables to calculate the impact of a 1% error in focal length. t = 19.95 m, f=1.274 m

Table 9. First relay, off-axis parabolas, inpact of a +1% focal length error.

OAP with error	OAP1 and 2	OAP1 only	OAP2 only
Shift in OAP1 (mm)	13.7	13.7	0
Ratio of new to old pupil size at DM	1.01	1.01	1
Shift in DM distance from OAP1 (mm)	13.7	13.7	0
Shift in OAP2 from DM (mm)	13.7	0	13.7
Ratio of output focal ratio to telescope's.	1	0.99	1.01

Table 10. Second relay, off-axis parabolas, inpact of a +1% focal length error

OAP with error	OAP1 and 2	OAP1 only	OAP2 only
Shift in OAP1 (mm)	3.2	3.2	0
Ratio of new to old pupil size at DM	1.01	1.01	1
Shift in DM distance from OAP1 (mm)	3.2	3.2	0
Shift in OAP2 from DM (mm)	11.1	0	11.1
Ratio of output focal ratio to telescope's.	1	0.99	1.01

5.1.2 Off-axis angle tolerance

Impact of an error in off-axis distance or angle, θ; angular error, $\Delta\theta$.

A. Identical error for both OAPs

First consider the case of an identical error for both OAPs. The first-order solution to minimizing the impact is to move the components to compensate for this error:

1. Ideally want to maintain the input and output beam directions. This requires that the first and second OAPs be tilted to the new angle with respect to these beams (i.e., OAP tilt = $\theta+\Delta\theta$).

   This is a tight constraint and somewhat unnecessary. We do have some freedom, but not much, to change the input and output beam direction via the tip/tilt mirror and science instrument location.

2. The DM must then be moved to the intersection of the beams from the two OAPs; it will be at the same angle with respect to both beams. It will need to be displaced

   $$\Delta x = t_{OAP1,DM}\cos\theta - t_{OAP1,DM}'\cos(\theta+\Delta\theta) \text{ and}$$

   $$\Delta y = t_{OAP1,DM}\sin\theta - t_{OAP1,DM}'\sin(\theta+\Delta\theta) ,$$

   where positive Δx and Δy are defined to be to the right and up, respectively, on Figure 5 (note that this is not the normal coordinate system definition for this figure).

3. The separation between the first OAP and the DM will now be

$$t_{OAP1,DM}' = t_{OAP1,DM} + \Delta\theta(t_{DM,OAP2}-t_{OAP1,DM}\cos\alpha)/\sin\alpha,$$

where α is the angle the center of the two OAPs subtend at the DM.

4. The separation between the DM and the second OAP will now be

$$t_{DM,OAP2}' = [t_{OAP1,DM}'\sin(\theta+\Delta\theta)-t_{OAP1,DM}\sin\theta+t_{DM,OAP2}\sin(\theta-\alpha)]/\sin(\theta-\alpha+\Delta\theta)$$

5. The pupil is located a distance $t_{OAP1,DM}' - t_{OAP1,DM}$ in front of the DM (i.e., toward OAP1). The change in distance from the pupil location to OAP2 is

$$\Delta s_2 = t_{DM,OAP2} - t_{DM,OAP2}' + t_{OAP1,DM} - t_{OAP1,DM}'$$

The distance from the focal plane to the exit pupil is

$$t' = [1/(-t_{DM,OAP2}+\Delta s_2)+1/f]^{-1} - f$$

B. OAP1 error only

Now consider the case of just the first OAP having an off-axis error.

1. We want to maintain the input and output beam directions. This requires that the first OAP be tilted to the new angle with respect to these beams (i.e., OAP tilt = θ+Δθ); while the second OAP is tilted to the nominal angle.

2. The DM must be moved to the intersection of the beams from the two OAPs; it moves along the line toward the second OAP by the amount $t_{DM,OAP2}-t_{DM,OAP2}'$; the equations in A.2. above are still valid.

3. The separation between the first OAP and the DM will now be

$$t_{OAP1,DM}' = t_{OAP1,DM} \sin\alpha/\sin(\alpha+\Delta\theta).$$

4. The separation between the DM and the second OAP will now be

$$t_{DM,OAP2}' = [t_{OAP1,DM}'\sin(\theta+\Delta\theta)-t_{OAP1,DM}\sin\theta+t_{DM,OAP2}\sin(\theta-\alpha)]/\sin(\theta-\alpha)$$

C. OAP2 error only

Now consider the case of just the second OAP having an off-axis error.

1. We want to maintain the input and output beam directions. This requires that the second OAP be tilted to the new angle with respect to these beams (i.e., OAP tilt = θ+Δθ); while the first OAP is tilted to the nominal angle.

2. The DM must be moved to the intersection of the beams from the two OAPs; it moves along the line to the first OAP by the amount $t_{OAP1,DM}$-$t_{OAP1,DM}$'; the equations in A.2 above are still valid.

3. The separation between the first OAP and the DM will now be

$$t_{OAP1,DM}' = t_{OAP1,DM} + t_{DM,OAP2}\Delta\theta/\sin(\alpha-\Delta\theta).$$

4. The separation between the DM and the second OAP will now be

$$t_{DM,OAP2}' = [t_{OAP1,DM}'\sin\theta - t_{OAP1,DM}\sin\theta + t_{DM,OAP2}\sin(\theta-\alpha)]/\sin(\theta-\alpha+\Delta\theta)$$

Summary: Using the first-order design values for the first relay ($t_{OAP1,DM}$ = 1.4595 m, $t_{DM,OAP2}$ = 1.366 m, θ = 25.0 deg., α = 20 deg., DM diameter=100mm):

Table 11. First relay off-axis parabolas, impact of a +0.1% error in off-axis angle. This corresponds to 1.5 arcmin delta angle

OAP with Error	OAP 1 and 2	OAP1 only	OAP2 only
Ratio of old to new OAP1 to DM distance	1.000	0.9988	1.0012
Ratio of old to new DM to OAP2 distance	0.9998	0.9986	1.0012
x-shift of beam at DM (mm)	0.3	1.9	-1.3
y-shift of beam at DM (mm)	-0.6	0.2	-1.3
Shift in pupil from DM (nn)	0.0	1.7	1.7
Size of pupil on DM (mm)	100	99.88	100.12
Location of exit pupil from OAP2 (m)	-8080	519	552

Table 12. First relay off-axis parabolas, impact of a +1% error in off-axis angle. This corresponds to 15 arcmin delta angle

OAP with Error	OAP 1 and 2	OAP1 only	OAP2 only
Ratio of old to new OAP1 to DM distance	1.000	0.9882	1.012
Ratio of old to new DM to OAP2 distance	0.9984	0.9865	1.012
x-shift of beam at DM (mm)	2.8	18.3	-13.2
y-shift of beam at DM (mm)	-5.7	1.6	-13.3
Shift in pupil from DM (nn)	0.1	17.3	17.6
Size of pupil on DM (mm)	99.995	98.8	101.2
Location of exit pupil from OAP2 (m)	-824	53.7	55.9

Because the above analysis assumes that we have maintained the input beam direction to OAP1 and the output beam direction from OAP2, we can treat the second relay as decoupled from the first. Thus all the above analysis applies to the second relay.

Table 13. Second relay off-axis parabolas, impact of a +0.1% error in off-axis angle. This corresponds to 0.78 arcmin delta angle

OAP with Error	OAP 1 and 2	OAP1 only	OAP2 only
Ratio of old to new OAP1 to DM distance	1.002	0.9994	1.0023
Ratio of old to new DM to OAP2 distance	1.000	0.998	1.0006
x-shift of beam at DM (mm)	-0.5	0.2	-0.7
y-shift of beam at DM (mm)	-0.2	0.0	-0.2
Shift in pupil from DM (nn)	0.5	0.2	0.7
Size of pupil on DM (mm)	24.039	23.985	24.054
Location of exit pupil from OAP2 (m)		2938.	865

Table 14. Second relay off-axis parabolas, impact of a +1% error in off-axis angle. This corresponds to 7.8 arcmin delta angle

OAP with Error	OAP 1 and 2	OAP1 only	OAP2 only
Ratio of old to new OAP1 to DM distance	1.016	0.9938	1.0227
Ratio of old to new DM to OAP2 distance	1.004	0.9981	1.0063
x-shift of beam at DM (mm)	-5.0	2.1	-7.1
y-shift of beam at DM (mm)	-1.9	-0.3	-2.4
Shift in pupil from DM (nn)	5.3	2.0	7.4
Size of pupil on DM (mm)	24.39	23.85	24.54
Location of exit pupil from OAP2 (m)	123	296	87

5.2 Zemax tolerancing analysis

Analysis of tolerances in the optical design were also done with the Zemax EE tolerancing tool. The tolerances analyzed can be divided into two categories: mounting tolerances essential for the mechanical design and manufacturing tolerances important for the vendors producing the optics. Included in the mounting tolerances are the tilt and decentration of the optical elements, as well as distances between them. The manufacturing tolerances concern the radii of curvature (for the powered optics), flatness (for the flat mirrors and dichroics) and off-axis angles (OAAs). The telescope was not included in the tolerancing.

Zemax allows tolerances to be evaluated by several different criteria. We have chosen the RMS wavefront error merit criteria, as this is directly comparable to values in the derived error budget. We've also performed a boresight criteria analysis, to ascertain stability requirements for the

optical mounts. The analysis was performed at 1 micron wavelength. Because of the difficulty in performing tolerance analyses on multi-configuration operands, the Zemax file was reduced to the science path configuration only (Figure 7). Tolerances may also be performed separately on the LGS WFS optical path, and the LOWFS, first relay if desired.

Compensators may also be defined in Zemax, and boundary values defined for the compensators. For these analyses we allowed compensation of the back focal distances of the first and seconds relays, with the boundary condition of +/- 10 mm. The compensators were optimized using orthogonal descent.

Initially, we performed a sensitivity analysis in which the change in merit criteria (RMS wavefront error or boresight) is calculated for each tolerance individually. This allows evaluation of the "worst offenders", indentifying which tolerances must be tightened, and which can be relaxed. An aggregate performance is estimated by a root square sum (RSS) calculation.

Once reasonable tolerances are determined using the sensitivity analysis, a Monte Carlo analysis simulates the effect of all the tolerance perturbations simultaneously. Zemax does this by assuming a normal distribution (modified Gaussian) of tolerance values within the user defined range of the tolerances. To provide adequate statistics, the Monte Carlo analysis was permitted to run n^2 times, where n is the number of individual tolerances.

5.3 Mounting Tolerances

Assembly tolerances resulting in acceptable performance of the NGAO relay are listed in Table 15. These tolerances are typical of standard assembly methods, and will not require extraordinary efforts to achieve.

Table 15. Mechanical tolerance values used in Zemax.

Parameter	Value	Units
Thickness (TTHI)	±0.200	mm
Decentration (TEDX/Y)	±0.100	mm
Element Tilt (TETX/Y)	±0.004	degrees

Thickness tolerances were applied to distances between optical elements, decentration was applied to OAPs, and tilt tolerances were applied to every optical element, including the OAPs, the DMs, the fold mirrors, and the dichroic beamsplitters.

The tilt and decenter of the K-mirror's individual mirrors, and the K-mirror unit as a whole, were included for completeness. However, the alignment and tolerancing of the K-mirror assembly, as it pertains to both pupil and image motion, has been analyzed in detail by previous generations of Keck optical engineers. This analysis is still pertinent, as the distance of the mirrors to focus is similar to the existing system (especially when compared to the 20 m distance to the exit pupil).

The subaperture width decreases by a factor of 60/20, and thus the tolerances to keep the pupil wandering less than 10% of a subaperture will be tighter by a factor of 3.

The sensitivity analysis indicates that the worst offenders are tilt errors in the low order DM (not surprisingly) and OAP mounts. However, a tilt of 0.004 degrees (14.2 arcseconds) at OAP1 results in less than a nanometer additional RMS wavefront error. Table 17 summarizes the worst offenders that had an appreciable effect on the RMS wavefront error.

Table 17. Worst offenders, mechanical tolerances

Tolerance	Value (degrees tilt)	Criterion (RMS WFE, nm,
TETY 19, LODM	0.004	22.1
TETY 19, LODM	-0.004	22.1
TETY 16, OAP1	-0.004	19.7
TETY 16, OAP1	0.004	19.7
TETY 27, OAP2	-0.004	19.7
TETY 27, OAP2	0.004	19.7

A Monte Carlo analysis of mounting errors leads to a similar conclusion. The nominal RMS wavefront error due to static aberrations for a perfectly aligned system is 18.8 nm (at 1 micron wavelength). For the tolerances listed in Table 15, a 2401 iteration Monte Carlo analysis predicts that 90% of the configurations will have less than 23.7 nm RMS wavefront error. This includes contributions from tilt error in the low order DM mount (which in practice will be mitigated by its attachment to the tip/tilt stage).

A boresight analysis was also performed to ensure that mechanical tilts and decenters resulted in movement on the camera of much less than a tenth of a pixel.

5.4 Manufacturing Tolerances

Considered separately are manufacturing tolerances to be specified to the vendor during procurement. These include tolerances on the radii of curvature for the OAPs, off-axis angles for the OAPs, flatness of the fold mirrors and dichroics, and figure errors for the OAPs. The off-axis nature of the OAPs led to difficulties in defining Zernike figure errors (i.e. the TEZI tolerance operand) because Zemax centered these aberrations on the parent parabola. Thus the figure errors for the OAPs will be considered with an analytic approximation outside of Zemax.

Table 19. Manufacturing Tolerances

Parameter	Value	Units
Radius (TRAD)	0.5%	Unitless
Flatness (TFRN)	±0.200	Fringes
Off-axis angle (TPAR)	$\pm 3.5 \times 10^{-5}$	Degrees

Table 19 details the manufacturing tolerances used in the Zemax analysis. The radius of curvature was assigned a tolerance of 0.5% of the radius, as given by Space Optics Research Labs (SORL) as a standard tolerance. The flatness of dichroics and folds was assumed to be within 0.200 fringes, as measured in a double pass Newton's rings type test. The off-axis angles (OAA) of the OAPs were given tolerances of 0.125 arcseconds, again as specified by Space Optics Research lab. The OAA tolerances were implemented by adjusting either the angle or off-

axis distance in the coordinate break preceding the OAP surface. Chief ray solves were left in during tolerancing to ensure that off-axis angles and off-axis distances were consistent.

The worst offenders were OAP tolerances for radii of curvature. Again, the nominal criteria for RMS wavefront error is 18.8 nm. A change of 0.5% in OAP1's radius of curvature corresponds to a 3 nm change in wavefront RMS. The back focal distances of relays 1 and 2 are allowed to change ±10mm in compensation. Table 20 summarizes the worst offenders that made an appreciable effect on the RMS wavefront error. If distance from Nasmyth focus to OAP1 had been allowed as a compensator (in effect, adjusting the position of the OAP to ensure that the optic produces a collimated beam) the criterion change is negligible. Likewise, for OAP3 if the distance from the 1st relay focus to OAP3 had been allowed as a compensator.

Table 20. Worst offenders, manufacturing tolerances.

Tolerance	Value	Criterion (RMS WFE,
TRAD 16, OAP1	6.8 mm	0.0221
TRAD 16, OAP1	-6.8 mm	0.0204
TRAD 34, OAP3	-1.75 mm	0.0189

A Monte Carlo simulation of manufacturing tolerances shows that these tolerances, like those adopted for mechanical mounting, are acceptable in terms of degradation to image quality. The 256 iteration Monte Carlo predicts that 90% of configurations will produce less that 20.5nm RMS wavefront error. The compensators in the Monte Carlo run had standard deviations which were 0.2% and 0.4% of the 1st relay back focal distance and 2nd relay back focal distance, respectively.

In support of the Error budget flowdown, and estimate of the correctable and uncorrectable wavefront errors due to manufacturing figure error was made. This worksheet can be found in

KAON 723, Performance Flowdown budgets spreadsheet. Table in Appendix lists the expected manufactured wavefront quality of the optics assumed for the Performance flowdown budget.

5.5 Thermal Tolerancing

The NGAO relay will be located in a temperature-controlled and cooled environment. A thermal analysis was performed in Zemax to ascertain the behavior of the optics as the bench is cooled from 20°C room temperature, to 0°C summit temperature, to -15°C of the cooled enclosure. The powered optics, the four OAPs, will change radius of curvature as the bench is cooled, and the bench itself will contract.

In Zemax the OAPs were assumed to be of Zerodur substrate with a CTE of 0.1 x 10^{-6} / °C, and the optical bench of stainless steel with a CTE of 12 x 10^{-6} / °C. Zemax thermal analysis is not applicable to decentered systems, so the effects of temperature change were evaluated with a single, on-axis parabola with the same radius of curvature as the parent parabola of the matched OAPs of the first relay.

Table 22. Thermal analysis of system cool-down

Temperature	20° C	0°C	-15°C
Radius of curvature (mm)	2553.493	2553.488	2553.484
Change in radius of curvature of OAP1, %	_	0.0001%	0.0003%
Contraction of optical bench over 1276.746 mm focal length of OAP1, (mm)	_	0.306	0.536
PV wavefront error (defocus) due to contraction of optical table (nm)		16	27

Table 22 shows the results of the thermal analysis for the OAP relays. The OAPs will change their radius of curvature by an amount that does not affect the wavefront error, even when uncompensated. The bench contraction, however, will introduce almost 30 nm of P-V wavefront error for each OAP. For four OAPs of the same focal length as OAP1 (root square summing the RMS wavefront errors, assuming the dominant error is defocus) the P-V wavefront error will be over 80 nm. Since OAP3 has a smaller focal length, by a factor of three, this represents an upper limit to the wavefront error caused by bench contraction.

There are a number of approaches to dealing with the thermal contraction of the bench. An Invar bench has a CTE ten times lower than that of stainless steel. The error could be precompensated for when aligning the bench at 0° C, given the design of the bench support structure.

6. Optical Design Summary

There are some aspects of the design and this document that are not complete for PDR.

- A section on alignment of the AO relay and an analysis of methods to pre-align the system given a cool-down of the optics enclosure from room temperature to -15 C.
- Specification of all coatings for the optics and windows are not yet complete.
- Polarization analysis of the system as it pertains to the interferometer will need to be performed.

The following table lists of each of the NGAO relay optics, giving figure, thickness, glass, and coating characteristics.

Table 23. Listing of NGAO relay optics

List of Optics, NGAO relay		transmissive	reflective		dichroic			
Science path	Diameter (mm)	thickness (mm)	Radius of curv. (mm)	Manufacturing quality	OAD (mm)	Substrate	Coating	λ T (transmit) or R (reflect)
Entrance window 1	180	25		λ/20		CaF2	sol gel ar	T 0.4-4.1μ
Entrance window 2	180	25		λ/20		CaF2	sol gel ar	T 0.4-4.1μ
K-mirror 1	250, long dir.			λ/20		Zerodur	lick	R 0.4-4.1μ
K-mirror 2	160, long dir			λ/20		Zerodur	lick	R 0.4-4.1μ
K-mirror 3	270, long dir			λ/20		Zerodur	lick	R 0.4-4.1μ
Fold mirror	200			λ/20		Zerodur	lick	R 0.4-4.1μ
OAP1	220		2553.493	λ/10	566.096	Zerodur	lick	R 0.4-4.1μ
Low-order DM	110						silver	R 0.4-4.1μ
LGS dichroic	190	20		λ/7		CaF2	dichroic	R 0.59-0.60μ T0.4-0.59μ, T0.6-4.1μ
OAP2	220		2553.493	λ/10	566.096	Zerodur	lick	R 0.4-4.1μ
IF dichroic	250	25		λ/7		CaF2	dichroic	R 1.0-4.1μ T0.4-1.0μ
Acq Cam dichroic	175	20		λ/7		CaF2	dichroic	R 0.4-0.6μ R 0.8-2.5μ T 0.6-0.8μ
Fold mirror	70x60			λ/20		Zerodur	lick	R 0.4-2.5μ
OAP3	70		635.975	λ/10	72.46	Zerodur	lick	R 0.4-2.5μ
High-order DM	25.6						silver	R 0.4-2.5μ
NGS dichroic	100	20		λ/7		CaF2	dichroic	R 0.4-0.8μ T 0.8-2.5μ
OAP4	150		1907.925	λ/10	731.005	Zerodur	gold	R 0.7-2.5μ
Fold mirror	150			λ/20		Zerodur	gold	R 0.7-2.5μ
LGS WFS path								
Fold mirror	250			λ/20		Zerodur		R 589 nm
Refocusing lens	250	30	940.381	λ/10		SF1	NA AR	T 589 nm
Refocusing lens	250	30	infinity	λ/10		SF1	NA AR	T 589 nm
Exit window 1	140	25		λ/20		BK7	NA AR	T 589 nm
Exit window 2	140	25		λ/20		BK7	NA AR	T 589 nm
NGS WFS path								
Triplet 1	100	20	-1320.064	λ/10		basf2	vis ar	T 0.4-0.8μ
			-1125.723	λ/10				
Triplet 2	100	17.5	305.403	λ/10		n15	vis ar	T 0.4-0.8μ
			-865.711	λ/10				
Triplet 3	100	20	-181.196	λ/10		basf2	vis ar	T 0.4-0.8μ
			-194.292	λ/10				
FSM 1	100			λ/20		Zerodur	Silver	R 0.4-0.8μ
	25			λ/20		Zerodur	silver	R 0.4-0.8μ

7. Mechanical Design – Overview

The AO sub-system (AO bench) consists of two optical relays in series for low and high order wave front correction. Several components providing functions for AO operation reside on the bench. However, laser guide star wave front sensing is done on a separately mounted subsystem (LGS WFS). The -15C operating temperature requires that the AO bench reside in a thermal enclosure. This enclosure has one entry port for light from the telescope and four exit ports. These exit ports feed 1) the science instrument (DAVINCI), 2) the dual star module (DSM) 3) the LGS WFS. The forth port is for a future "round two" instrument (I2). Figure 32 shows the AO bench and surrounding systems in the intended location on the nasmyth platform. Figure 33 details the components of the bench. The following sections describe the AO bench in its preliminary design.

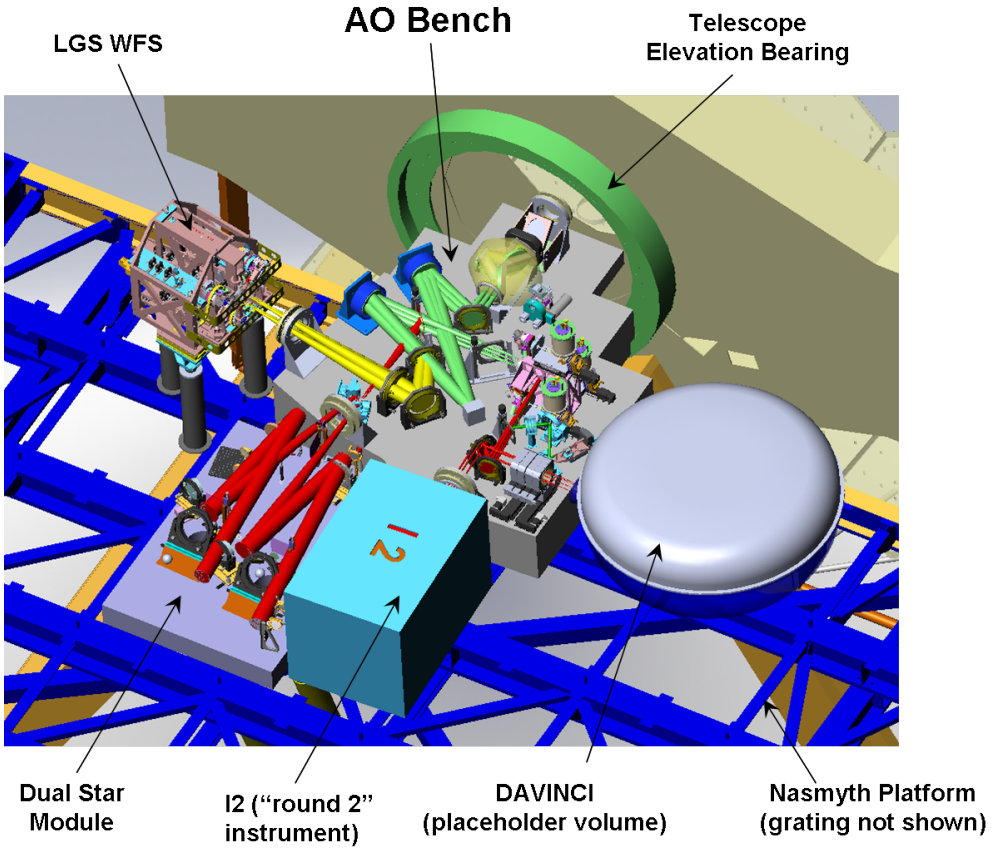

Figure 32. NGAO - AO Bench and Related Systems (Note: several components are suppressed to expose detail, i.e. the cold enclosure for AO Bench, external enclosure for entire system, and the calibration system.)

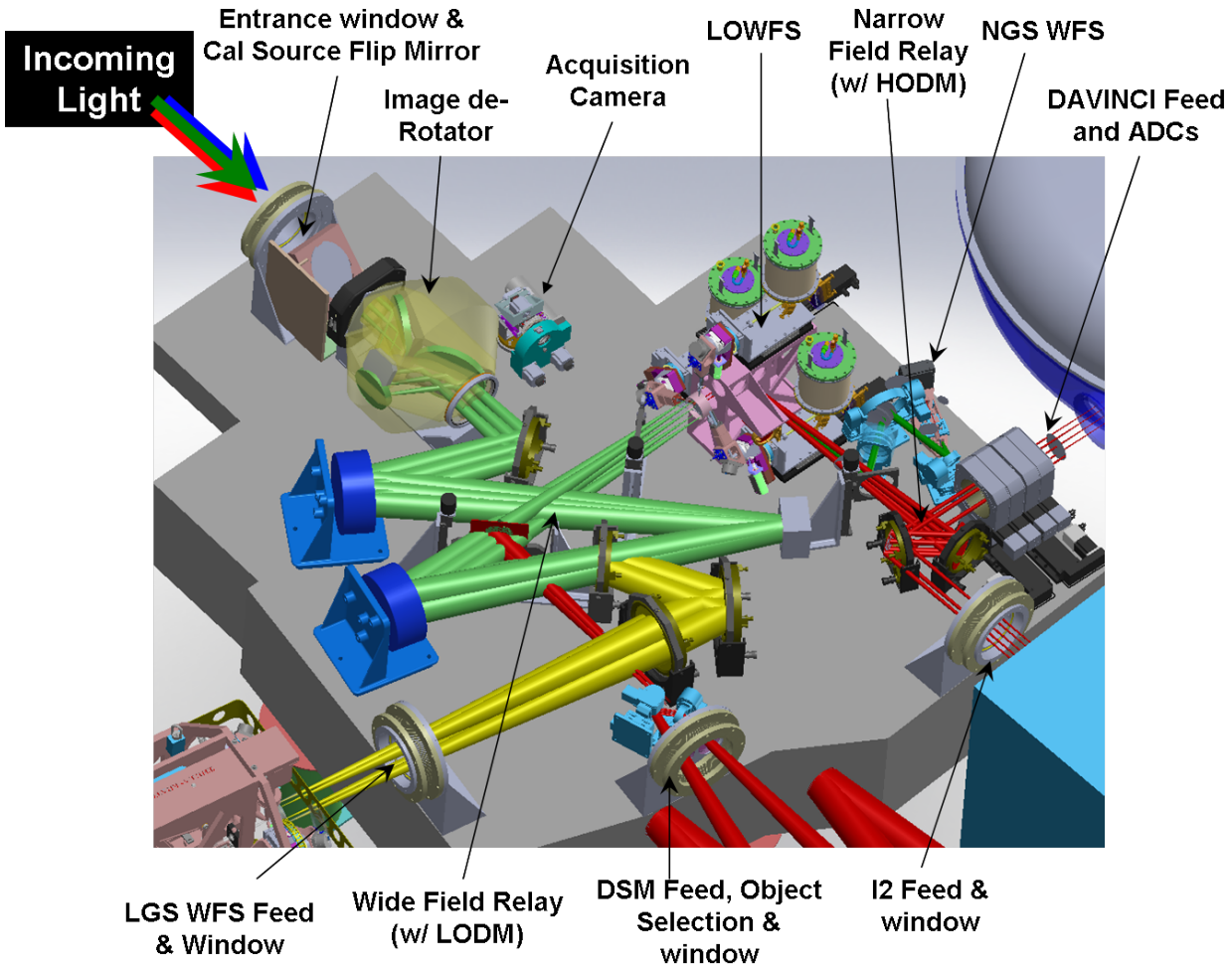

Figure 33. AO Bench Components

8. Sub System Description

8.1 Image De-Rotator

The K-mirror de-rotator of the current Keck AO system is the base line design for NGAO. The internal and external alignment specification for the existing rotator is 10 arcsec (KAON 093). The specification for the new rotator will scale with the spatial frequency resolution of the deformable mirrors. I.e. alignment requirements for the new rotator are 3 times more stringent or ~ 3arcsec. (Note that up to the sensitivity of adjustments, once-per-rev nutation can be corrected. However, this is not true for radial run out of higher frequency.) Since acceptable performance for the existing rotator has been challenging, we are intending to actively drive the gimbal mounted fold mirror that directly follows the rotator so as to relax these alignment requirements. The tip/tilt motion of this fold mirror can be used to re-steer the pupil as described in the Wide Field Relay section below.

The tracking requirements are currently driven by the needs of the interferometer in Dual-Star mode: 50 microradians of field rotation (D.Gavel memo “AO Subsystem Alignment Stability”

4/16/10). The drive for the rotator is an Aerotech rotary stage – ALAR-150-LP (http://www.aerotech.com/products/stages/alarspecs.html). This is a direct drive stage with a 150 mm clear aperture, an accuracy spec of 19 microradians, and a tilt error spec listed at 10 microradians. The bearing opposite the drive stage will be a preloaded cross roller ring - THK RA15008 (150mm clear aperture also).

Detailed Design phase will require fleshing out 3 mirror cells and support structure. The three cells and support structure will require tip/tilt adjustment and kinematic definition. The rotator is represented below in Figure 34.

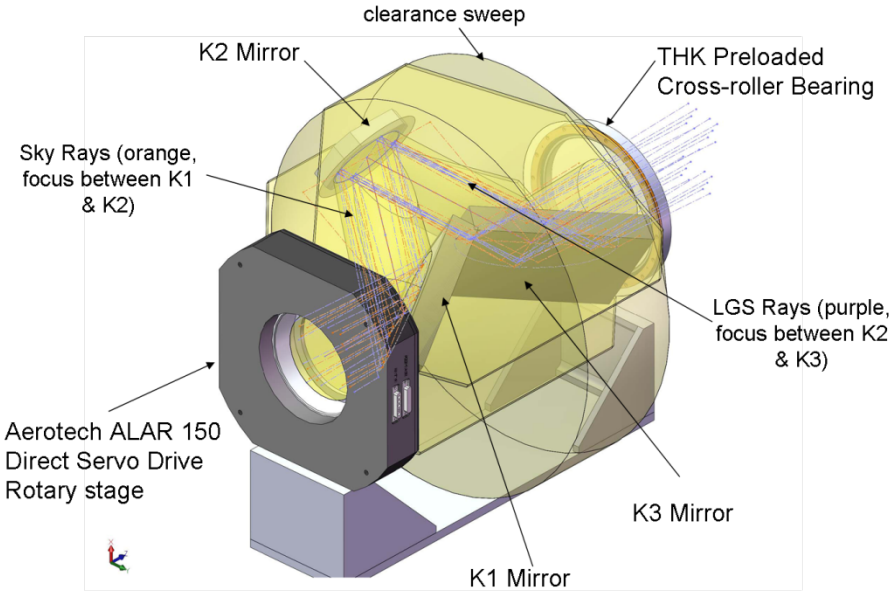

Figure 34. Image De-rotator w/Aerotech direct drive rotary servo stage.

8.2 Wide Field Relay

Light exits the de-rotator and travels thru the wide field relay which places the pupil on the LODM. Tip/tilt correction will also be made at this pupil, therefore the LODM will be mounted in a fast tip/tilt stage. Cilas corporation has provided ROM estimates for a LODM and integral tip/tilt stage based on similar units they have designed and manufactured, however the particular stage for NGAO has not yet been designed in detail, so the form volume has only been estimated, with no detail existing yet in our CAD model.

The Wide Field Relay is shown in Figure 35.

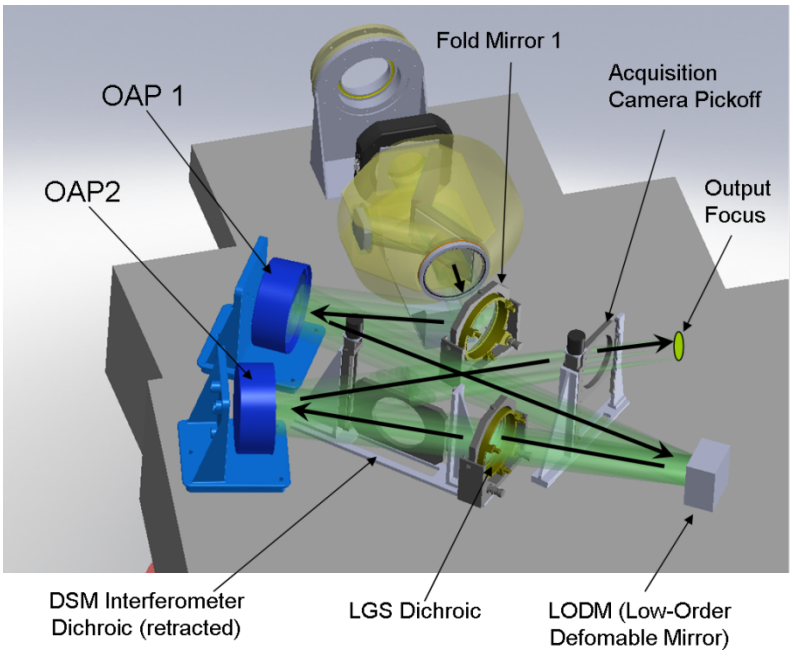

Figure 35. Wide Field Relay (shown with de-rotator for reference)

Fold Mirror 1 – As mention previously slow tip/tilt steering correction due to misalignment of the de-rotator is planned for the first fold mirror. This functionality was incorporated late in this design phase and no detail exists as yet. However this can have closed-loop operation based on feedback of pupil illumination information from a wavefront sensor. Stroke will be less ≤ 1deg. Resolution requirement will be on the order of 1 arcsec. This has typically been done with a high resolution load encoding on a (commercial if possible) gimbal mount using geared, servo plunger actuators. We have yet to find this niche filled by a commercial vendor. However we have produced similar retrofits previously.

Siko (http://www.sikoproducts.com/MagLine/Incremental) is a source for sub-micron incremental encoders. They use magnetic poles and thus require no light source like some competing products. Unfortunately they are rated only to -10 C whereas we will need a -15 C operation. The (unofficial) word from the manufacturer is that this is a limitation due to the flex cable insulation brittleness at low temperature. As long as the cable is not bending in cable wrap it will operate at much lower temperatures.

OAP1 and 2 – As a baseline for PD we are using SORL commercial OAP mounts. This assumes the mounting features that they use in the optics.

LODM and Fast Tip/Tilt Stage – Vendor Supplied (http://www.cilas.com/adaptative-mirrors.htm). See the discussion in Section 3.4.

LGS Dichroic – This is a fixed Aerotech 10inch gimble mount (http://www.aerotech.com/products/optmnts/aom110.html).

DSM Dichroic – This will be a THK LM stage. Its ball screw driven shaft encoding only required (in or out, motion parallel to planar surfaces). Custom cell for optic and vertical mount will be required.

Acquisition Pickoff – We had planned for this to be identical to the the DSM dichroic stage. (We recently discovered this pickoff may need a third position: to allow a mirror as well as a dichroic. The solution for a 3 position stage would be to use a vertical transport stage. We would also need to have the optics oval to minimize their dimension normal to the table in order to allow room to stow one below the beam.)

8.3 Narrow Field Relay (and LOWFS)

The Wide Field Relay terminates at a focus with a 120 arcsec/100 mm diameter field. An outer annulus is patrolled by the LOWFS pick offs. An inner 60 arcsec/30 mm diameter field is passed thru to Fold Mirror 2. It proceeds into the Narrow Field Relay where the pupil is placed on the HODM. The Narrow Field Relay is shown below in Figure 36.

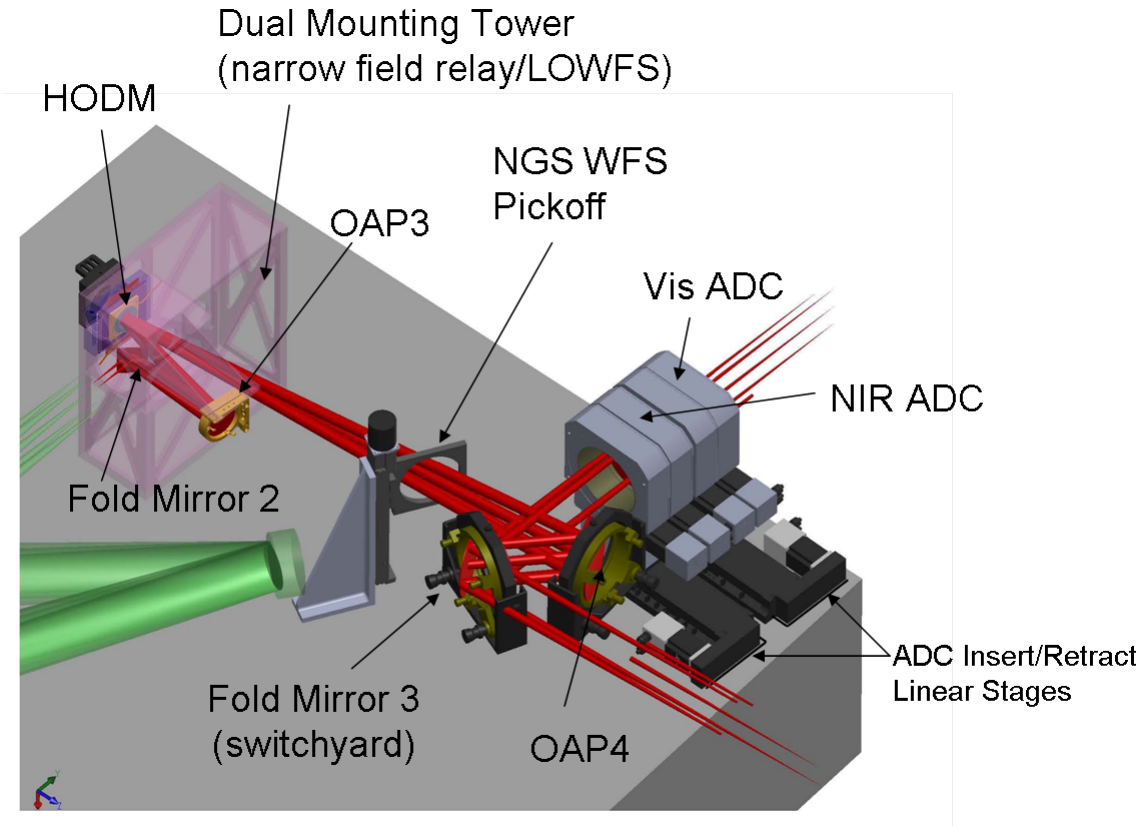

Figure 36. Narrow Field Relay (Note the dual mounting tower shown in pink is transparent to show detail. Three LOWFS channels are installed after the Narrow Field Relay)

The first three elements of the Narrow Field Relay (Fold Mirror 2, OAP3, HODM) are closely located with the LOWFS assembly. Figure 37 shows this tight packaging.

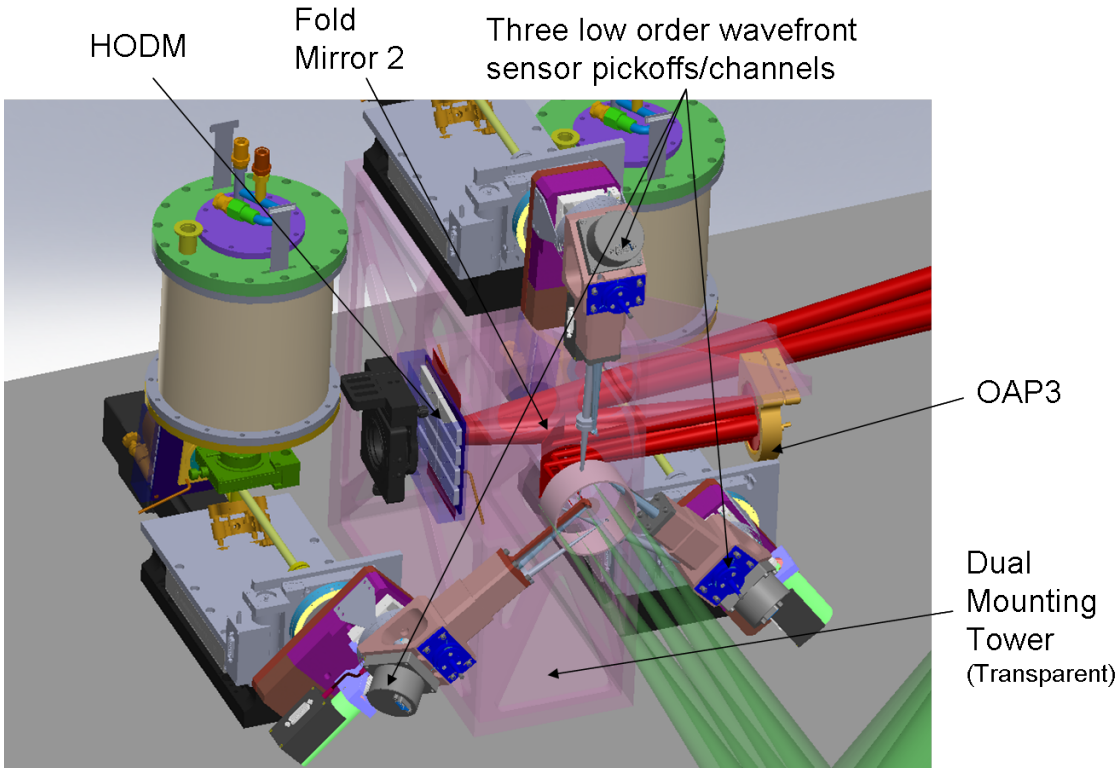

Figure 37. Initial Narrow Field Relay components with surrounding LOWFS channels

Fold Mirror 2 – This mount requires manual fine tip/tilt adjustment. We have not identified the solution for this mount yet but expect this to be specialized as the beam returning from OAP3 comes close to this mirror. The mechanism will be displaced below the mirror to avoid vignetting the return beam. A rotary stage mounted on a goniometer is the current idea.

OAP 3 – The off-axis angle of this OAP is quite shallow. As such a simple kinematic mirror mount may suffice (we show a Newport kinematic mount). There is space available to accommodate purpose built commercial or custom mount.

HODM Tip/Tilt – The functional requirements for this motorized slow tip/tilt stage are developed in KAON 669. Requirements are similar to the 1st fold mirror of the wide field relay. The stroke required is > 0.5 degrees while the resolution is an arcsec or better. Again, this has been done with a high resolution load encoding on a (commercial if possible) gimbal mount using geared, servo plunger actuators. Piezo driven, flexured tip/tilt stages exceed the resolution requirements but lack the travel. (Piezo power consumption is also a concern.)

NGS Dichroic – Similar to the dichroic stages on the wide field relay, a THK LM stage is planned. Its ball screw driven, requiring shaft encoding only (in or out, motion parallel to planar surfaces). Custom cell for optic and vertical mount will be required.

OAP4 – We show a standard 4inch gimbal mount. This optic will however, require a purpose built solution. The beam must pass on either side of OAP4 in order to feed a second instrument. It must also pass as close as possible to the OAP to minimize the path length consumed. Therefore volume occupied by the mount outside the perimeter of the OAP must be minimized.

Switchyard Mirror – This is a flat fold that sends light to the science instrument. A retrofit is envisioned that allows the mirror to swing out and feed light to a second instrument. This capability incorporated in a subsequent development effort. Thus, it is currently static and mounted in a 4 inch gimbal.

ADCs – Two atmospheric dispersion correctors are required to cover the visible and infrared spectral bands served to the science instruments. Each ADC requires three degrees-of-freedom 1) counter rotation to correct color 2) collective rotation to match horizon 3) insertion/retraction. None of these has challenging accuracy requirements. The solutions shown have two worm drive stages each, mounted on a ball screw driven, linear ball bearing translation stage. All stages here are Aerotech.

8.4 LGS Light and DSM Light

The sodium dichroic for the laser guide star light is in the collimated beam just after the LODM. The light is reflected of Fold Mirror 3, sent thru a focusing lens and the exit window to the LGS WFS as shown in Figure 38. The three optics are mounted in 10-inch Aerotech gimbal mounts, all of which remain fixed.

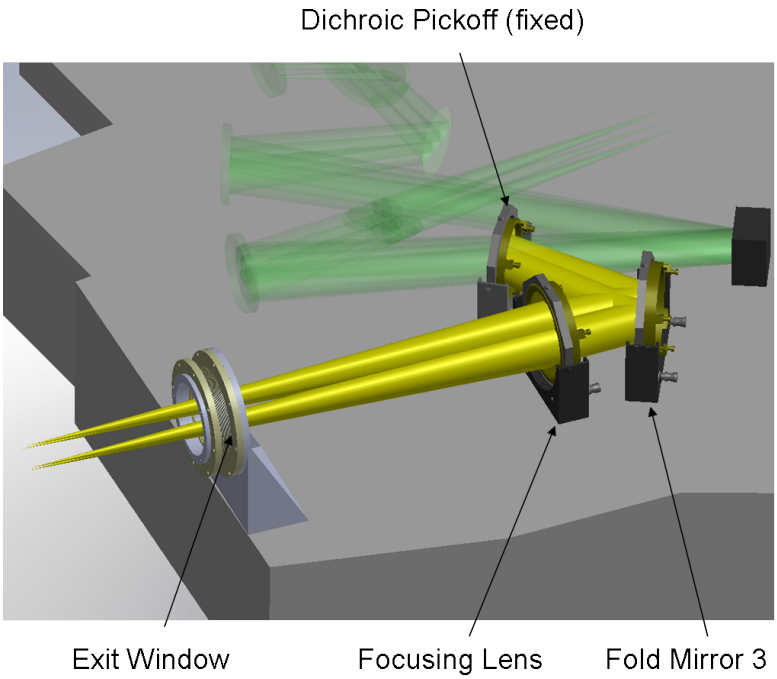

Figure 38. Laser Guide Star Beam and Optical Components (Note that all elements are static mounts once aligned. DSM light, object selection components, and window are suppressed in this view. As such it appears more spacious than it is. This can be seen in the next figure.)

8.5 Interferometer Pickoff and Object Selection

Figure 39 below shows the LGS Light with the Dual Star Module Interferometer light added in. The DSM dichroic can be retracted down and out of the beam. This mechanism is described in Wide Field Relay section.

Object Selection Pair – Two servo driven gimbals are used here. They are Newmark stages with 5 arcsec repeatability.

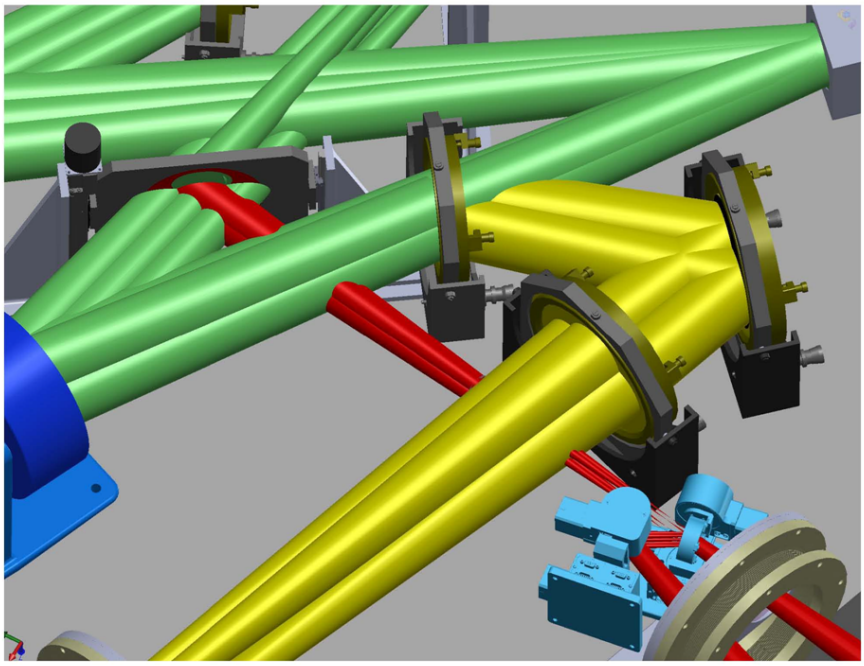

Figure 39. DSM Light (red) and DSM Selection Pair

8.6 Entry and Exit Windows

The entry and exit widows demark the interface of the of the thermal enclosure design to the bench. The tilt requirements on the windows relative to the optical paths demand they be mounted solidly to the table. They must also be sealed to the inside wall of the thermal enclosure. However they must be mechanically decoupled from the walls for stability. The windows are double-paned with dry gas fill in the gap to preclude condensation and provide insulation. An insulated flex-bellows will couple window mount to the enclosure wall (Figure 40).

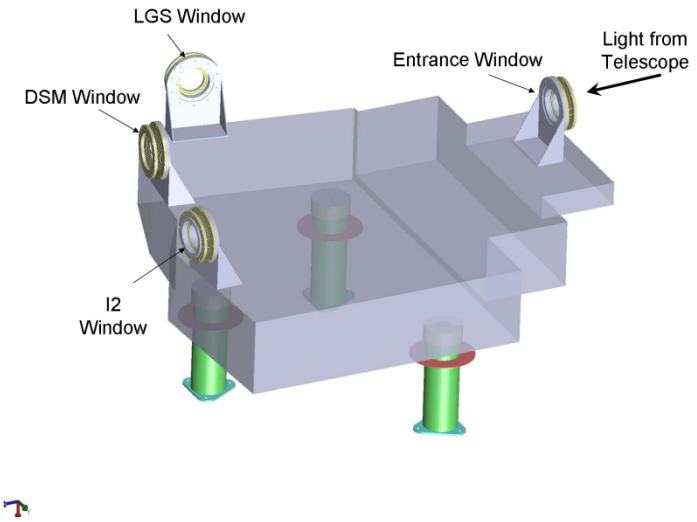

Figure 40. Window Locations on the AO Bench

9. Support Structure Mounting Alignment and Stability

9.1 Optical Table

The components described above will be mounted on an optical table of sandwich-construction – top and bottom face sheets and honeycomb core. As mentioned, the AO Bench will be housed in a thermal enclosure to reduce temperature of the optics to -15 C for reduced emissivity. The plan-form of the table will be a custom shape to both minimize the volume of the thermal enclosure and provide edges normal to the entry and exit beams.

The bench materials still need to be specified. Selection will depend on alignment sensitivities. The AO bench will be aligned at telescope dome temperature prior to cooling. We will assume that the bench once cooled in the enclosure will be at isothermal conditions. Therefore to first order, contraction in the optical table will shrink the layout of the bench, but not change the geometry. That is to say the impact will be primarily separation of optical surfaces and not decenter or steering. (Note this is for on-board components of the bench. External Optical interfaces are discussed below.) The exact impact of thermal contraction will be evaluated in detailed design phase. The standards are 400 series stainless steel face sheets with steel

honeycomb core. Invar skins can be ordered for lower coefficient of thermal expansion (contraction).

Table thickness will be driven by compliance, payload and support configuration. Thorough mass estimates are required for this analysis. This will also be done in detailed design phase.

9.2 Kinematic Mount

The bench will be mounted supported similar to the current system, on three legs with kinematic mount features – cone, V-groove and flat, and mating spheres. Figure 41 shows an example of one of these features. The legs are grounded to the nasmyth platform, which is steel and presumably tracking dome temperature. The AO bench and kinematic interfaces are at -15C. Therefore, for the legs to remain un-sprung from lateral loads in the legs (caused by relative thermal expansion of platform and table - and friction in the kinematics) explicit degrees-of-freedom will be built into the V-groove (1DOF) and flat (2DOF). This will be done using rolling elements or flexures (not shown in the figure). The reason this will be important is explained in the next section.

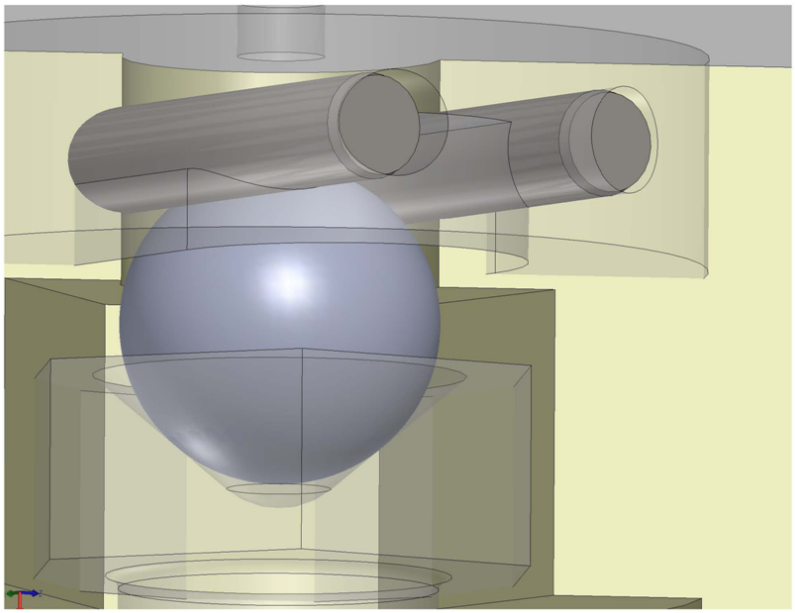

Figure 41. Kinematic Mount Feature Example (V-groove equivalent)

9.3 External Optical Interface Stability (Horizontal Plane)

If, as mentioned, explicit degrees of freedom are built into the kinematics for the AO bench, and the surrounding components are similarly mounted, then it is possible to limit the motion of the surrounding components (relative to the bench) to focus motion only. This is the best we can do without passive compensators or active control. We think it is good enough since these are slow f/# beams and consequently the depth of focus is soft.

Assume that the nasmyth platform behaves isothermally (no significant gradients). For thermal expansion/contraction then, all points move radially toward/away from **any** reference point. Therefore the kinematic cones of all the components – the points anchored to the platform – move relative to each other on the axis that contains them.

Figure 42 is a top-down view showing the cone position on the AO bench on the optical axis of the telescope. In theory this means it can only move in focus (toward/away from the tertiary mirror of the telescope). The bench cone is also coincident with the DAVINCI science instrument optical axis. If the cone for DAVINCI support is also placed on its own optical axis the relative motion due to expansion of the platform is restricted along the focus direction of the instrument.

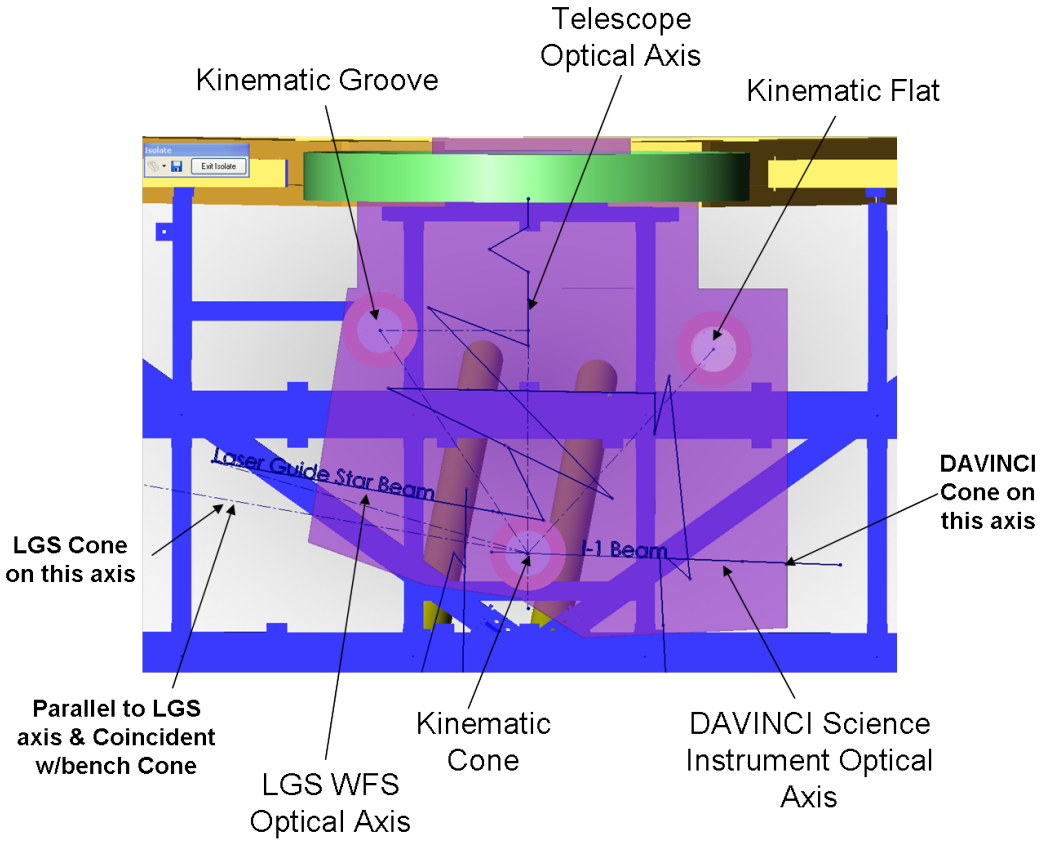

Figure 42. Plan View of AO bench Optical Table (transparent purple) showing location of legs, gut ray traces and optical axes

The LGS Optical axis however does not intersect the telescope axis at the same location as DAVINCI's axis does. We can place the cone for the LGS WFS on the axis parallel its optical axis and coincident with the bench cone and achieve the same desired effect of thermal expansion /contraction along the focus direction.

It is important to arrange for this system of kinematic positioning of disparate support cones. Otherwise, if there were some angle between the optical axis and the axis between bench/instrument cones features, then a sine component of decenter would be induced by temperature fluctuations. The decenter stability requirement for DAVINCI is a tight 5 microns. For perspective, 5 microns is the sine component induced by a 2 degree C change in platform temperature given a 1500 mm cone separation if the cone to optical axis angle is, for example, 18 degrees.

10. AO Subsystem Alignment Stability

This section provides a rough guidance on how well the alignment must remain stable between the AO optical table and ancillary subsystems that are not mounted to this table, during the course of an AO-corrected science exposure. The subsystems can drift with respect to each other for various reasons but perhaps the most important one is the fact that the steel Nasmyth platform to which they are all mounted will be subject to the ambient temperature fluctuations in the dome.

Four subsystems receive output beams from the AO system: the laser guidestar wavefront sensor unit, the two science instruments, and the interferometer. Also the AO system receives an input beam from the telescope at its Nasmyth focus.

10.1 Starting Assumptions

We assume that each optical interface from subsystem to AO system is defined by the co-orientation of beam lines. The beam-line orientation is defined by six degrees of freedom: three positions (x, y, z) where z is along the beam and x and y are orthogonal to it, and three orientation angles (θx, θy, θz) where θz is the clocking rotation around the z axis. For simplicity, we'll define each interface at point that corresponds to an intermediate focus position.

10.2 Stability Requirements

10.2.1 Science Instruments

The science instruments will see the beam after it is corrected by AO and tip/tilt. Furthermore there is no automatic adjustment of position or focus available for the science instrument. Therefore, the stability requirements are the strictest here.

Lateral position (x, y) must be kept to a small fraction of diffraction-limited.

Focus (z) must be kept to within a small fraction of depth of focus.

Angle (θx, θy) must be such that pupil shift is less than a small fraction of a Hartmann subaperture.

Clocking (θz) must be such that rotation of the field blurs a star at the edge of the field by less than the diffraction limit.

The table below summarizes the requirements, giving representative numbers.

Table 24. Stability of science instrument interfaces at f/46.3

Degree of freedom	Criterion	Tolerance required
x, y	Diffraction limit / 10	4.6 micron
z	Depth of focus / 10	200 microns
θx, θy	15 cm subap / 10	32 micro radians
θz	Diffraction limit 20 arcsec off-axis / 10	100 micro radians

10.2.2 Laser guidestar wavefront sensor unit

The laser guidestar wavefront sees the beam after it has been corrected by the woofer and fast tip/tilt. However, the sensor is insensitive to tip/tilt in regards to the quality of the corrected beam going to the science instrument. It only needs to stay within its own range of capture to be able to run the local tip/tilt loops to keep the spots centered in the Hartmann subapertures.

Lateral position (x, y) must be kept within a fraction of the tip/tilt dynamic range.

Focus (z) must be kept to a small fraction of the range of the wavefront sensor. It is assumed that the common slow focus term measured in these sensors is compensated by the focus term measured by the truth wavefront sensor.

Angle (θx, θy) must be such that pupil shift is less than a small fraction of a Hartmann subaperture.

Clocking (θz) must be such that rotation of the field blurs a star at the edge of the field by less than the capture range of the off-axis HOWFS tip/tilt dynamic range.

The table below summarizes the requirements, giving representative numbers.

Table 25. Stability of LWS WFS interface at f/13.5 (plate scale = 0.74 mm/arcsec)

Degree of freedom	Criterion	Tolerance required
x, y	~ 0.1 arcsec on sky	65 microns
z	~0.1 arcsec spot deflection at outer subaperture	2 mm
θx, θy	15 cm subap / 10	110 micro radians
θz	~0.1 arcsec at 10 arcsec off-	10 milliradian

	axis radius	

10.2.3 Interferometer feed

The interferometer feed is derived via a beam splitter that is located in the f/13.5 output space of the first AO relay. It comes to a focus at a pinhole in the star selection mirror of the dual star module. Both the star selection mirror and a subsequent beam steering mirror are mounted on the AO table, however the rest of the dual star module optics are on a separate optical bench. To specify stability we will refer to the above mentioned focal point. A mental picture is that the co-stability of the DSM to the AO bench must be such that a hypothetical beam coming from the DSM (light travelling in reverse) comes to focus at the star selection mirror pinhole.

Lateral position (x, y) must be kept within a fraction of the tip/tilt dynamic range of the interferometer, or the diameter of the pinhole, whichever is smallest.

Focus (z) must be kept within the dynamic range of the interferometer fringe tracker, and small enough that the defocused beam gets through the pinhole diameter.

Angle (θx, θy) must be such that pupil shift is less than a small fraction of a Hartmann subaperture. The idea here is that light that does not overlap at pupil images in the interferometer will not interfere, resulting in loss of light for the interferometer science.

Clocking (θz) must be such that rotation of the field blurs a star at the edge of the interferometer field by less than a fraction of the interferometer diffraction-limit (lambda/baseline). The interferometer field is set by the maximum range of the DSM for the off-axis star (I'm assuming this is roughly an isoplanatic angle ~10 arcsec).

The table below summarizes the requirements, giving representative numbers.

Table 26. Stability of Interferometer interface at f/13.5

Degree of freedom	Criterion	Tolerance required
x, y	~0.1 arcsec on sky	65 microns
z	range of fringe tracker, perhaps 2 mm?	2 mm
θx, θy	15 cm subap / 10	110 micro radians
θz	10 arcsec fov x clock angle < difrac lim /10. (difrac lim = 2.5 mas)	50 micro radians

10.2.4 Telescope input at Nasmyth focus

The telescope provides the input beam to the AO system. Since this beam is in the common path ahead of the AO system, the tolerance on pointing stability is no more than that of acquisition into the AO system. The pupil centering stability is not terribly critical either, except that a mismatch of the Keck pupil with its mapping onto the AO system's pupil images (assuming they are all perfectly aligned with each other) may result in some degraded correction around the edge. Also, the first turning mirror in the first AO relay could be motorized to adjust the centering based on a feedback from the wavefront sensor on how evenly the subapertures are illuminated.

Lateral position (x, y) must be kept within the range of the tip/tilt mirror.

Focus (z) must be kept within the dynamic range of the truth wavefront sensor over a period of time comparable to the telescope focus offload cycle.

Angle (θx, θy) must be such that pupil shift is less than a small fraction of a telescope pupil, again, over a period of time comparable to the centering offload cycle.

Clocking (θz) must be such that rotation of the field blurs a star at the edge of the interferometer field by less than a fraction of the interferometer diffraction-limit (lambda/baseline). This is the tightest requirement demanded by a downstream instrument and is assumed to apply until a twist component sensed by the LOWFS can be offloaded to the K-mirror derotator.

Table 27. Stability of Telescope interface at f/13.7

Degree of freedom	Criterion	Tolerance required
x, y	~1 arcsec on sky	725 microns
z	range of TWFS /10	2 mm
θx, θy	10 m aperture / 100	1000 micro radians
θz	10 arcsec fov x clock angle < difrac lim /10. (difrac lim = 2.5 mas)	50 micro radians

Table of Figures

Table of Tables